JOURNAL OF GEOPHYSICAL RESEARCH, VOL. 113, D05213, doi:10.1029/2007JD009258, 2008

Using aircraft measurements to estimate the magnitude and uncertainty of the shortwave direct radiative forcing of southern African biomass burning aerosol

Brian I. Magi,[1,2] Qiang Fu,[1] Jens Redemann,[3] and Beat Schmid[4]

Received 6 August 2007; revised 30 October 2007; accepted 12 December 2007; published 13 March 2008.

[1] We estimate the shortwave, diurnally averaged direct radiative forcing (RF) in cloud-free conditions of the biomass burning aerosol characterized by measurements made from the University of Washington (UW) research aircraft during the Southern African Regional Science Initiative in August and September 2000 (SAFARI-2000). We describe the methodology used to arrive at the best estimates of the measurement-based RF and discuss the confidence intervals of the estimates of RF that arise from uncertainties in measurements and assumptions necessary to describe the aerosol optical properties. We apply the methodology to the UW aircraft vertical profiles and estimate that the top of the atmosphere RF (RF_{toa}) ranges from -1.5 ± 3.2 to -14.4 ± 3.5 W m^{-2}, while the surface RF (RF_{sfc}) ranges from -10.5 ± 2.4 to -81.3 ± 7.5 W m^{-2}. These estimates imply that the aerosol RF of the atmosphere (RF_{atm}) ranges from 5.0 ± 2.3 to 73.3 ± 11.0 W m^{-2}. We compare some of our estimates to RF estimated using Aerosol Robotic Network (AERONET) aerosol optical properties and show that the agreement is good for RF_{toa}, but poor for RF_{sfc}. We also show that linear models accurately describe the relationship of RF with the aerosol optical depth at a wavelength of 550 nm (τ_{550}). This relationship is known as the radiative forcing efficiency (RFE) and we find that RF_{toa} (unlike RF_{atm} and RF_{sfc}) depends not only on variations in τ_{550}, but that the linear model itself is dependent on the magnitude of τ_{550}. We then apply the models for RFE to daily τ_{550} derived from the Moderate Resolution Imaging Spectroradiometer (MODIS) satellite to estimate the RF over southern Africa from March 2000 to December 2006. Using the combination of UW and MODIS data, we find that the annual RF_{toa}, RF_{atm}, and RF_{sfc} over the region is -4.7 ± 2.7 W m^{-2}, 11.4 ± 5.7 W m^{-2}, and -18.3 ± 5.8 W m^{-2}, respectively.

Citation: Magi, B. I., Q. Fu, J. Redemann, and B. Schmid (2008), Using aircraft measurements to estimate the magnitude and uncertainty of the shortwave direct radiative forcing of southern African biomass burning aerosol, *J. Geophys. Res.*, *113*, D05213, doi:10.1029/2007JD009258.

1. Introduction

[2] The radiative properties of an atmospheric aerosol are dependent on the aerosol chemical composition [*Jacobson*, 2001; *Chung and Seinfeld*, 2005], the chemical mixing state [*Ackerman and Toon*, 1981; *Chylek et al.*, 1988], and the physical size distribution of the particles that make up the aerosol [*Seinfeld and Pandis*, 1998]. The radiative impact of an aerosol is often quantified by the radiative forcing which is the difference in the net flux at some point in the atmosphere (usually at the top of the atmosphere or at the surface) with and without the aerosol in question [e.g., *Ramaswamy et al.*, 2001]. On a global scale, radiative forcing by aerosols is estimated using chemical transport models and general circulation models [*Jacobson*, 2001; *Chung et al.*, 2005; *Reddy et al.*, 2005a], but such simulations need to be either tied to observations [*Christopher et al.*, 2000; *Abel et al.*, 2005; *Chung et al.*, 2005; *Reddy et al.*, 2005a] or validated by observations [*Ginoux et al.*, 2006]. Regardless of the methods, uncertainties in aerosol radiative forcing that arise from both the measurements and from the assumptions needed to properly describe unmeasured aerosol optical properties are difficult to quantify [*Redemann et al.*, 2000; *McComiskey et al.*, 2008] and generally require sensitivity studies. The lack of precise knowledge about aerosol properties, and therefore the radiative impact of aerosols, hampers model predictions of the future climate [*Anderson et al.*, 2003a; *Schwartz*, 2004; *Andreae et al.*, 2005; *Delworth et al.*, 2005].

[3] A number of field campaigns designed to characterize aerosol properties in different locations around the world have helped address the uncertainties [*Reid et al.*, 1998; *Clarke et al.*, 2002; *Russell et al.*, 2002; *Swap et al.*, 2003;

[1]Department of Atmospheric Sciences, University of Washington, Seattle, Washington, USA.
[2]Now at Atmospheric and Oceanic Sciences Program, Princeton University, Princeton, New Jersey, USA.
[3]Bay Area Environmental Research Institute, Sonoma, California, USA.
[4]Pacific Northwest National Laboratory, Richland, Washington, USA.

0148-0227/08/2007JD009258$09.00

Doherty et al., 2005; *Magi et al.*, 2005; *Quinn and Bates*, 2005; *Redemann et al.*, 2006; *Schmid et al.*, 2006]. In situ measurements in the field campaigns often include some or all of the properties described below. The wavelength-dependent (subscript "λ" notation) extinction ($\sigma_{ext,\lambda}$), scattering ($\sigma_{sca,\lambda}$), and absorption ($\sigma_{abs,\lambda}$) coefficients are basic properties of an aerosol that have a good history of measurements and are all dependent on the aerosol number concentration (N_a). Values of $\sigma_{ext,\lambda}$ can be determined by adding $\sigma_{sca,\lambda}$ and $\sigma_{abs,\lambda}$, and the wavelength-dependent aerosol optical depth (τ_λ) can be calculated by integrating $\sigma_{ext,\lambda}$ over specific vertical limits [e.g., *Hartley and Hobbs*, 2001; *Magi et al.*, 2003]. Properties that are not dependent on N_a are the wavelength-dependent single scattering albedo ($\omega_{o,\lambda} = \sigma_{sca,\lambda}/\sigma_{ext,\lambda}$), backscatter ratio ($\beta_\lambda$), and asymmetry parameter (g_λ). The wavelength dependence of $\sigma_{ext,\lambda}$, $\sigma_{sca,\lambda}$, and $\sigma_{abs,\lambda}$ can be described using the respective Angstrom exponents ($\alpha_{ext,\lambda}$, $\alpha_{sca,\lambda}$, and $\alpha_{abs,\lambda}$), which are defined as the slopes of the optical properties with respect to wavelength on log-log scale (such that, for example, $\sigma_{ext,\lambda} \sim \lambda^{\alpha_{ext,\lambda}}$). All the terms discussed above have been defined by, for example, *Seinfeld and Pandis* [1998], and the notation in this study is the same as in the companion study by *Magi et al.* [2007].

[4] In this study, we estimate the diurnally averaged, shortwave radiative forcing (henceforth, simply RF) of southern African biomass burning aerosol in cloud-free (clear sky) conditions at the top of the atmosphere, by the atmosphere, and at the surface (RF_{toa}, RF_{atm}, and RF_{sfc}, respectively) using aerosol optical properties obtained during the Southern African Regional Science Initiative field campaign [*Swap et al.*, 2003] in August and September 2000 (SAFARI-2000) by the University of Washington (UW) research aircraft [*Hobbs et al.*, 2003; *Magi et al.*, 2003; *Schmid et al.*, 2003; *Sinha et al.*, 2003a]. We describe the methods and assumptions we use to compile the input to the radiative transfer model in section 2. We discuss our methods of estimating uncertainty in RF in section 3 and present our best estimates of RF in section 4. We then describe the linear models of the radiative forcing efficiency (RF/τ_{550}) in section 4 and apply the models to 6 years of τ_{550} measured by the Moderate Resolution Imaging Spectroradiometer (MODIS) satellite over the southern African region to derive a general picture of RF over the region. Throughout section 4, we compare our estimates with values derived from Aerosol Robotic Network (AERONET) data products and with past studies of the radiative impact of the southern African aerosol.

2. Methods

[5] We use the Fu-Liou radiative transfer model (RTM) to estimate the diurnally averaged radiative fluxes in a cloud-free atmosphere with and without a polluted aerosol layer that is characterized by measurements obtained in southern Africa during the SAFARI-2000 dry season campaign. This RTM has been extensively documented [*Liou et al.*, 1988; *Fu and Liou*, 1992] and has been used to study the radiative effects of aerosols [e.g., *Liao and Seinfeld*, 1998; *Christopher et al.*, 2000; *Redemann et al.*, 2000; *Hansell et al.*, 2003; *Yu et al.*, 2004; *Zhou et al.*, 2005]. We use the delta-four-stream approximation in the model to calculate radiative fluxes in an atmosphere with the aerosol properties measured during SAFARI-2000 [*Magi et al.*, 2003]. The shortwave spectrum in the RTM is partitioned into ten discrete wavelength bands from 175 to 700 nm and five bands from 700 to 4000 nm. The longwave optical properties of biomass burning particles [e.g., *Jacobson*, 2001; *Reddy et al.*, 2005b] are not addressed in this study. Additional details about the flux calculations are described in Appendix A.

[6] To compile shortwave aerosol optical properties that characterize the southern African atmosphere for input to the RTM, we use a retrieval methodology described by *Magi et al.* [2007] together with measurements of aerosol properties obtained from the UW research aircraft during SAFARI-2000 [*Magi et al.*, 2003]. Briefly, the retrieval methodology is based on Mie theory and finds a submicron aerosol size distribution and spectral refractive index that together reproduce available measurements of aerosol optical properties (namely, σ_{ext} and ω_o) within measurement uncertainties. Using this "optically equivalent" size distribution and spectral refractive index from the retrieval, we can derive a complete set of aerosol optical properties that are closely tied to actual observations. *Magi et al.* [2007] provide a full description of the retrieval, including limitations in the applicability, while additional details related to the assumptions used in this study are described in Appendix A.

[7] We assume that most of the biomass burning particles are confined below ~500 hPa and can be represented by the retrieved aerosol optical properties, while above ~500 hPa, we assume that τ_{550} exponentially decreases to values described by *Vanhellemont et al.* [2005] and other aerosol optical properties are from *Fenn et al.* [1985]. This assumption is consistent with climatologies of the vertical structure of the southern African atmosphere [*Cosijn and Tyson*, 1996; *Garstang et al.*, 1996; *Swap and Tyson*, 1999] and with data collected during SAFARI-2000 [*Haywood et al.*, 2003a, 2003b; *McGill et al.*, 2003; *Magi et al.*, 2003; *Schmid et al.*, 2003]. For the spectral surface albedo (ρ), we use measurements made during SAFARI-2000 by the NASA Cloud-Absorption Radiometer (CAR) on the UW research aircraft when available [*Gatebe et al.*, 2003] and the MODIS (Moderate Resolution Imaging Spectroradiometer) satellite white-sky surface albedo product [*Moody et al.*, 2005] otherwise. The differences between the MODIS white-sky and the black-sky albedo products are minimized since we only examine and report diurnally averaged RF [*Yu et al.*, 2004].

3. Uncertainty

[8] Estimates of diurnally averaged RF at the different levels in the atmosphere (RF_{toa}, RF_{atm}, and RF_{sfc}) are better understood if accompanied by estimates of the uncertainty in RF (δRF). However, since the radiative transfer equation is solved by numerical integration, δRF cannot be calculated using the standard quadratures method of error propagation. We therefore estimate δRF by exploring the sensitivity of RF to variations in the input. Using the Fu-Liou RTM, we first calculate RF for the base case scenario (which provides the central estimate) and we then recalculate RF after independently varying σ_{ext}, ω_o, g, and ρ. We assume that

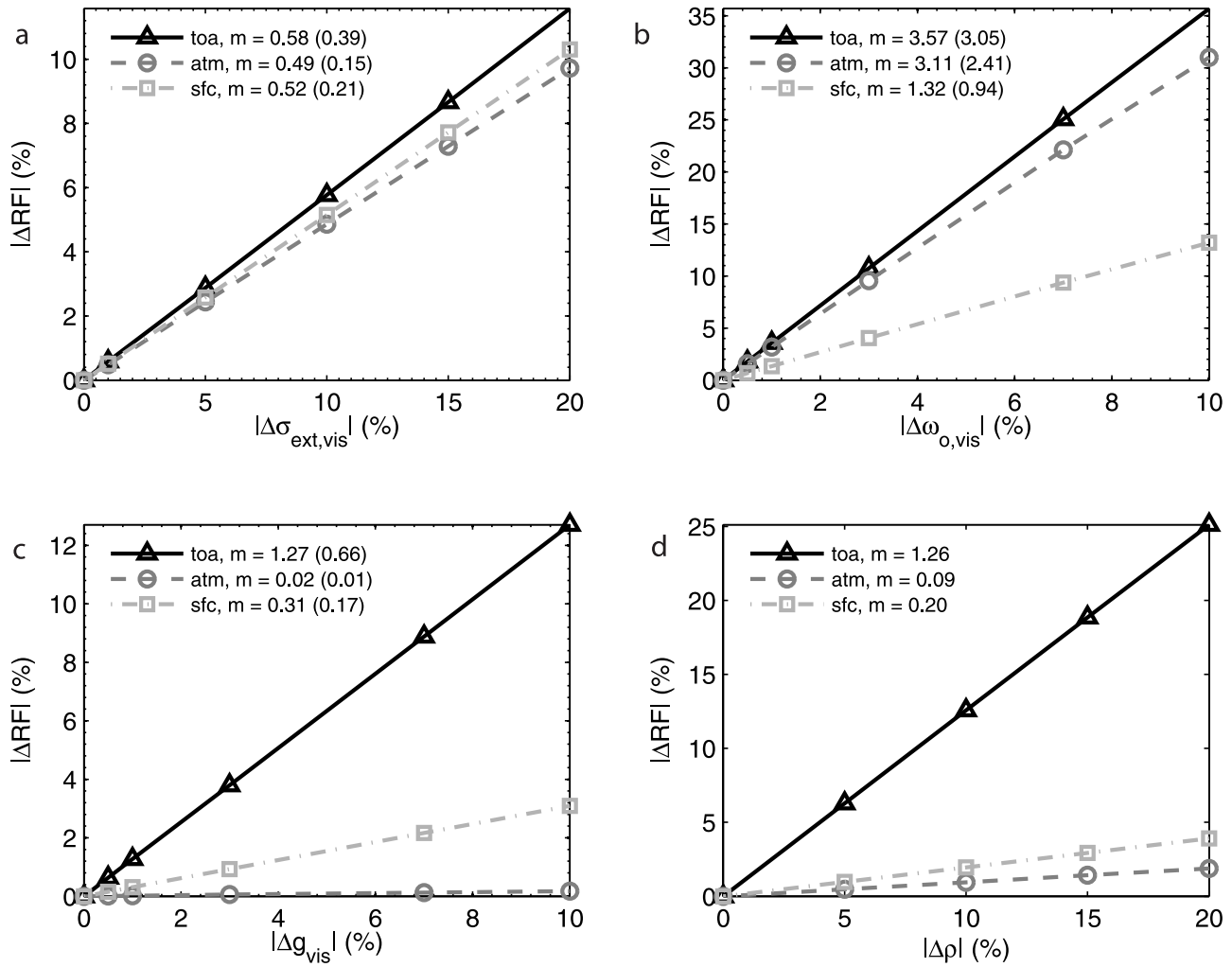

Figure 1. The absolute percent change of radiative forcing ($|\Delta RF|$) to (a) absolute percent changes in visible wavelength (400–700 nm) aerosol extinction coefficient ($|\Delta\sigma_{ext,vis}|$), (b) single scattering albedo ($|\Delta\omega_{o,vis}|$), and (c) aerosol asymmetry parameter ($|\Delta g_{vis}|$) and to (d) absolute percent changes in surface albedo ($|\rho|$). The base case is a 0% change. The slopes (m) of the values of $|\Delta RF|$ at the top of the atmosphere (toa, solid line with triangles), by the atmosphere (atm, dashed line with circles), and at the surface (sfc, dash-dotted line with squares) are given in each part. Larger values of m indicate a greater sensitivity of RF. The values of m for $|\Delta RF|$ as a function of changes in nonvisible wavelength (200–400 nm and 700–4000 nm) aerosol optical properties are given in parentheses for comparison (the curves are not shown).

these particular properties account for most of δRF, but acknowledge that uncertainties in various other input to the RTM may play a role. We then apply the general results of these sensitivity tests to specific uncertainties in σ_{ext}, ω_o, g, and ρ to arrive at the final estimate of δRF. The approach we adopt is similar to techniques used in other studies to estimate δRF [*Liao and Seinfeld*, 1998; *Redemann et al.*, 2000; *McComiskey et al.*, 2008].

[9] We set up the sensitivity tests by calculating the percent change in RF (ΔRF_{toa}, ΔRF_{atm}, and ΔRF_{sfc}) versus the percent that we vary the particular property ($\Delta\sigma_{ext}$, $\Delta\omega_o$ and Δg, and $\Delta\rho$). We vary the values of σ_{ext} and ρ by as much as ±20% around the base case values, and we vary the values of ω_o and g by as much as ±10% around the base case values (imposing the physical restriction of $0 < \omega_o < 1$ and $-1 < g < 1$). The imposed ranges adequately encompass the real uncertainties in the particular properties, which we return to later in this section. In all cases, as we move away from the base case value, the magnitudes of ΔRF_{toa}, ΔRF_{atm}, and ΔRF_{sfc} will also increase, noting that the rate of increase (i.e., the sensitivity) depends on which property is varied and on the base case value of that property.

[10] In Figure 1, we show the relationships of the absolute values of ΔRF_{toa}, ΔRF_{atm}, and ΔRF_{sfc} ($|\Delta RF_{toa}|$, $|\Delta RF_{atm}|$, and $|\Delta RF_{sfc}|$) to the absolute values of $\Delta\sigma_{ext}$, $\Delta\omega_o$, Δg, and $\Delta\rho$ ($|\Delta\sigma_{ext}|$, $|\Delta\omega_o|$, $|\Delta g|$, and $|\Delta\rho|$). In Figures 1a–1c, we show the sensitivity of RF to changes in visible wavelength (λ = 400–700 nm) values of σ_{ext}, ω_o, and g ($|\Delta\sigma_{ext,vis}|$, $|\Delta\omega_{o,vis}|$, and $|\Delta g_{vis}|$), but we discuss the sensitivity of RF to $\Delta\sigma_{ext}$, $\Delta\omega_o$, and Δg for all shortwave wavelengths in the text. Note also that the absolute values of variations in ρ ($|\Delta\rho|$) are presented in terms of the entire

Table 1. Descriptions of the University of Washington Research Aircraft Vertical Profiles Obtained During the SAFARI-2000 Field Campaign[a]

Date (2000)	Latitude,[b] °S	Longitude,[b] °E	UTC Time, hhmm	Altitude,[c] km	τ_{550}	$\omega_{o,550}$	g_{550}	ρ_{550}	RF_{toa}, W m^{-2}	RF_{atm}, W m^{-2}	RF_{sfc}, W m^{-2}
14 Aug	25.90 ± 0.09	27.89 ± 0.04	1114–1126	1.44–3.56	0.22	0.88	0.51	0.08	−7.1 ± 2.4	12.3 ± 3.1	−19.3 ± 2.7
14 Aug	25.48 ± 0.30	27.68 ± 0.19	1228–1247	1.45–3.71	0.35	0.91	0.53	0.07	−11.8 ± 2.6	12.5 ± 3.4	−24.3 ± 2.9
17 Aug	24.06 ± 0.16	29.75 ± 0.21	0708–0725	1.28–3.21	0.17	0.89	0.57	0.08	−4.7 ± 2.7	7.7 ± 2.4	−12.4 ± 2.4
20 Aug	23.95 ± 0.08	29.01 ± 0.27	1132–1146	1.59–3.72	0.16	0.92	0.57	0.08	−5.5 ± 2.3	5.0 ± 2.3	−10.5 ± 2.4
22 Aug	24.98 ± 0.04	31.61 ± 0.06	0816–1006	0.37–3.82	0.36	0.91	0.57	0.08	−9.1 ± 2.7	14.9 ± 3.6	−24.1 ± 3.0
24 Aug	25.98 ± 0.03	32.91 ± 0.02	0810–0824	0.21–4.12	0.29	0.87	0.61	0.07	−7.9 ± 2.7	17.5 ± 4.3	−25.4 ± 3.6
29 Aug	23.10 ± 0.15	28.82 ± 0.08	1030–1047	1.65–3.77	0.19	0.91	0.56	0.08	−6.0 ± 2.4	8.3 ± 2.7	−14.3 ± 2.5
31 Aug	21.62 ± 0.17	34.27 ± 0.13	1229–1244	0.64–3.89	0.33	0.84	0.50	0.06	−8.6 ± 2.8	21.5 ± 4.9	−30.1 ± 3.9
1 Sep	17.48 ± 0.13	25.09 ± 0.02	1051–1059	2.15–3.77	0.23	0.87	0.51	0.08	−6.2 ± 2.7	14.6 ± 3.6	−20.8 ± 3.4
2 Sep	19.89 ± 0.02	23.55 ± 0.02	0952–1009	1.12–4.42	0.33	0.85	0.48	0.09	−6.5 ± 2.8	23.7 ± 4.7	−30.2 ± 3.7
3 Sep	20.59 ± 0.03	26.17 ± 0.02	0831–0850	1.08–4.58	0.80	0.84	0.54	0.09	−9.4 ± 4.7	52.2 ± 9.5	−61.6 ± 6.7
3 Sep	20.56 ± 0.07	25.90 ± 0.02	1012–1035	0.99–4.57	0.65	0.81	0.52	0.09	−7.0 ± 3.9	50.4 ± 7.5	−57.4 ± 5.5
6 Sep	16.24 ± 0.11	23.42 ± 0.12	0746–0755	1.23–3.79	1.13	0.83	0.59	0.08	−8.0 ± 4.0	72.4 ± 12.4	−80.4 ± 8.7
6 Sep	15.19 ± 0.05	23.16 ± 0.03	0917–0929	1.37–4.77	1.12	0.83	0.58	0.08	−8.8 ± 4.8	72.5 ± 10.8	−81.3 ± 7.5
6 Sep	15.31 ± 0.08	23.11 ± 0.05	0934–0950	1.65–4.77	1.11	0.83	0.58	0.09	−7.9 ± 5.9	73.3 ± 11.0	−81.2 ± 7.8
6 Sep	15.47 ± 0.22	23.46 ± 0.16	0957–1014	1.64–5.27	1.07	0.84	0.60	0.08	−9.9 ± 5.2	68.5 ± 10.6	−78.4 ± 7.5
7 Sep	23.61 ± 0.03	31.12 ± 0.19	1135–1147	1.25–4.10	0.25	0.93	0.63	0.07	−6.8 ± 2.5	9.5 ± 2.7	−16.3 ± 2.7
11 Sep	21.99 ± 0.11	12.39 ± 0.07	0925–0933	0.75–3.76	0.45	0.86	0.63	0.04	−14.4 ± 3.5	22.9 ± 4.7	−37.2 ± 4.7
13 Sep	20.24 ± 0.05	13.22 ± 0.02	1116–1135	1.02–5.10	0.52	0.88	0.58	0.18	−3.6 ± 5.6	31.6 ± 6.1	−35.2 ± 4.2
16 Sep	19.19 ± 0.04	15.84 ± 0.04	1052–1107	1.35–4.76	0.30	0.89	0.62	0.19	−1.5 ± 3.2	17.2 ± 3.7	−18.7 ± 2.8

[a]Also listed are properties at a wavelength of 550 nm, which include the column aerosol optical depth (τ_{550}), single scattering albedo ($\omega_{o,550}$), asymmetry parameter (g_{550}), and the surface albedo (ρ_{550}) used in the radiative transfer model to estimate shortwave, diurnally averaged radiative forcing (RF) at the top of the atmosphere (RF_{toa}), atmosphere (RF_{atm}), and surface (RF_{sfc}) under cloud-free conditions. Values of $\omega_{o,550}$ and g_{550} are extinction-weighted column averages.

[b]These are the mean ± standard deviation of the latitude and longitude during the period of the vertical profile.

[c]Altitude is above mean sea level; the surface elevation in southern Africa varies.

shortwave spectrum in Figure 1d. The slopes listed in Figure 1 represent the linear regression to the average of the individual cases (i.e., the 20 UW vertical profiles), the slopes of which vary around this average linear regression. The intercepts are all very close to zero (ranging from −0.019 to 0.021, and median of −0.00015) and the linear correlation coefficients (r^2) are all very close to one (median value is 0.98), so are not explicitly listed. The general interpretation of Figure 1 is that a larger slope implies a greater sensitivity of RF to the particular property ($\sigma_{ext,vis}$, $\omega_{o,vis}$ and g_{vis}, and ρ).

[11] The sensitivity of RF to visible wavelength aerosol optical properties (Figures 1a–1c) and the shortwave surface albedo (Figure 1d) changes depending on which part of the atmosphere (top of the atmosphere, atmosphere, or surface) we examine. In a percentage sense, the slopes for RF_{toa} (black lines with triangles in Figure 1) are consistently greater than the slopes of RF_{atm} and RF_{sfc}, which implies that RF_{toa} is more sensitive to changes in visible wavelength aerosol optical properties and shortwave surface albedo. In this study, this is mainly because the magnitudes of the actual RF_{toa} are much smaller than the magnitudes of RF_{atm} and RF_{sfc} (Table 1 and section 4), but also emphasizes how uncertainties affect the estimates of RF_{toa}, RF_{atm}, and RF_{sfc} differently. In decreasing order, RF_{toa} is most sensitive to $\omega_{o,vis}$, g_{vis}, ρ, and $\sigma_{ext,vis}$. The order changes to $\omega_{o,vis}$, $\sigma_{ext,vis}$, g_{vis}, and ρ for RF_{sfc}, while for RF_{atm}, the order is $\omega_{o,vis}$, $\sigma_{ext,vis}$, ρ, and g_{vis}, noting that RF_{atm} exhibits very little sensitivity to ρ and g_{vis}. RF at all levels is much more sensitive to $\omega_{o,vis}$ than to $\sigma_{ext,vis}$, g_{vis}, and ρ.

[12] The sensitivity of RF to changes in the nonvisible wavelength (λ = 200–400 nm and λ = 700–4000 nm) aerosol optical properties is similar, but the nonvisible slopes (shown parenthetically in Figure 1) are about 54%, 22%, and 48% less than those of $\sigma_{ext,vis}$, $\omega_{o,vis}$, and g_{vis}, respectively. The fact that shortwave RF is less sensitive to nonvisible wavelength aerosol optical properties follows from the fact that the solar spectrum peaks in the visible and the small particles associated with biomass burning emissions [e.g., *Reid et al.*, 2005a] interact most strongly with solar radiation near the peak of the spectrum. Regardless of the smaller sensitivity of RF to variations in nonvisible aerosol optical properties, RF is still much more sensitive to nonvisible wavelength ω_o than it is to σ_{ext}, g, and ρ over any wavelength range, but the sensitivity of RF to nonvisible wavelength ω_o is about 22% less than the sensitivity of RF to $\omega_{o,vis}$.

[13] The most important thing to notice is that regardless of the wavelengths, RF in an overall sense is most sensitive to ω_o. Other studies have pointed out that ω_o is the critical parameter in characterizing an aerosol [e.g., *Redemann et al.*, 2000; *Russell et al.*, 2002; *Abel et al.*, 2005], but here we quantify the sensitivity and suggest that RF is a factor of ~6.2 times more sensitive to $\omega_{o,vis}$ than to $\sigma_{ext,vis}$, g_{vis}, and ρ, and ~4.7 times more sensitive to nonvisible wavelength ω_o than to $\sigma_{ext,vis}$, g_{vis}, and ρ. The sensitivity of RF to $\sigma_{ext,vis}$ is consistent throughout the atmosphere (i.e., similar slopes in Figure 1a), and generally smaller for $\sigma_{ext,nonvis}$. The sensitivity of RF to g_{vis}, g_{nonvis}, and ρ suggests that these quantities are most crucial when estimating RF_{toa}, and less crucial when estimating RF_{atm} and RF_{sfc}. The fact that RF is less sensitive to g (visible or nonvisible wavelengths) than other optical properties has also been pointed out in past studies [e.g., *Pilewskie et al.*, 2003; *Zhou et al.*, 2005]. The caveat to this sensitivity study is that we are looking at the sensitivity of RF to the specific ranges of shortwave ω_o and

ρ listed in Table 1. The range of ρ considered in this study is typical of land surfaces around the world [e.g., *Moody et al.*, 2005], while the aerosol absorption is moderate to high compared to other regions of the world [e.g., *Dubovik et al.*, 2002].

[14] To translate the sensitivities of RF to the properties described above and in Figure 1 into estimates of δRF, we first derive uncertainties in the aerosol optical properties ($\delta\sigma_{ext}$, $\delta\omega_o$, δg) and surface albedo ($\delta\rho$). Values of $\delta\rho$ are estimated to be ±10% on the basis of our qualitative assessment of the range of values described by *Gatebe et al.* [2003] and the spatial variability of the MODIS white-sky surface albedo product [*Moody et al.*, 2005]. Median values of $\delta\sigma_{ext}$, $\delta\omega_o$, and δg are ±9%, ±5%, and ±4%, respectively, and are derived by combining measurement uncertainties associated with each aerosol optical property [*Magi et al.*, 2003; *Magi*, 2006] and structural uncertainties in the retrieval we used to retrieve the shortwave optical properties [*Magi et al.*, 2007].

[15] However, because we impose an assumption of the wavelength dependence of ω_o based on commonly cited aerosol climatologies published by *d'Almeida et al.* [1991] and *Hess et al.* [1998], values of $\delta\omega_o$ at nonvisible wavelengths are subject to greater uncertainty than that which arises from measurements uncertainties and structural uncertainties alone. We use a linear combination of soot and continental aerosol types [*d'Almeida et al.*, 1991] to represent the base case in our RF calculations, but as described by *Magi et al.* [2007, Figure 3], there are many possible options for the assumption of the wavelength dependence of ω_o [*d'Almeida et al.*, 1991; *Ross et al.*, 1998; *Bergstrom et al.*, 2003; *Pilewskie et al.*, 2003], none of which are strongly supported by quantitative field data [e.g., *Bond and Bergstrom*, 2006]. Although there is evidence of internal mixing [*Ackerman and Toon*, 1981; *Chylek et al.*, 1988] of different chemical species in the southern African biomass burning particles [*Li et al.*, 2003; *Posfai et al.*, 2003], we only attempt to model the particles as an external (linear) mixture of soot and continental aerosol. The retrieval [*Magi et al.*, 2007] matches measured aerosol optical properties to optical properties calculated using standard Mie theory, so although one could argue that an internal mixture might be more representative of biomass burning particles [*Reid et al.*, 2005a, 2005b], the results of the retrieval are closely tied to real physical measurements regardless of the chemical mixing state.

[16] To account for the additional uncertainty associated with the assumption of the wavelength dependence of ω_o, we calculate RF for every constraint on ω_o shown by *Magi et al.* [2007, Figure 3] applied to every individual case presented in this study. This provides us with a range of RF values that bracket the base case scenario of an external mixture of soot and continental aerosols. We suggest that half the full range of calculated RF (using all the different constraints on ω_o for each of the 20 vertical profiles) is the uncertainty in RF associated with the constraint on ω_o. These uncertainties (i.e., ±range/2) vary from ±3 to 29% in RF_{toa}, ±4 to 14% for RF_{atm}, and ±2 to 4% for RF_{sfc}, with the median values equal to ±11% for RF_{toa}, ±5% for RF_{atm}, and ±2% for RF_{sfc}. For comparison, the median uncertainties in RF that results from uncertainty in visible wavelength ω_o (~3–6% and derived mainly from measurement uncertainty) are ±18% for RF_{toa}, ±16% for RF_{atm}, and ±7% for RF_{sfc}.

[17] Finally, we use the values of $\delta\sigma_{ext}$, $\delta\omega_o$, δg, and $\delta\rho$ as the independent variables in the linear regressions to arrive at the estimate of δRF due to the uncertainty in each aerosol optical property and in the surface albedo. We use the linear regression coefficients for each individual case (not listed) as opposed to the linear regression coefficients shown in Figure 1, because the linear regression (i.e., the sensitivity of RF) is dependent on the base case values of the aerosol optical properties and the surface albedo for the particular case (see values at $\lambda = 550$ nm in Table 1). We combine the errors using a standard quadratures methods (i.e., $\delta RF^2 = \delta\sigma_{ext}^2 + \delta\omega_o^2 + \delta g^2 + \delta\rho^2$), and also include the estimate of uncertainty in the flux calculations of the Fu-Liou RTM of ±2 W m^{-2} discussed in Appendix A. As implied in the sensitivity tests (Figure 1), we ignore the cross-correlated terms in the estimation of uncertainty.

[18] If we examine the apportionment of the total uncertainty, the median contributions of $\delta\omega_o$ to δRF_{toa}, δRF_{atm}, and δRF_{sfc} (with respect to the uncertainty in RF due to $\delta\sigma_{ext}$, $\delta\omega_o$, δg, and $\delta\rho$) are 57%, 92%, and 58%, respectively, where we calculate the apportionment in terms of the variances (for example, $100 * \delta\omega_o^2/\delta RF_{toa}^2 = 57\%$). The vast majority (92%) of δRF_{atm} is due to $\delta\omega_o$, while the remaining 8% is due to $\delta\sigma_{ext}$. Values of $\delta\sigma_{ext}$, δg, and $\delta\rho$ are the remaining terms contributing to δRF with ranges of 8–36%, 0–3%, and 0.3–14%, respectively. The second largest contributions to δRF_{sfc} are due to $\delta\sigma_{ext}$, while for δRF_{toa}, uncertainties in ρ are the second largest contributor. Looking more closely at $\delta\omega_o$, we find that the average contribution of uncertainties in visible wavelength ω_o dominate the overall uncertainty in ω_o, contributing on average between 64 and 87%. This strongly supports the notion that better measurements [e.g., *Sheridan et al.*, 2005; *Sierau et al.*, 2006] and a more complete understanding [*Ackerman and Toon*, 1981; *Chylek et al.*, 1988; *Jacobson*, 2001; *Bond and Bergstrom*, 2006] of aerosol absorption are needed to improve estimates of aerosol RF. Even focusing on reducing uncertainties in the visible wavelength ω_o would be very useful to reducing uncertainties in the global estimates of aerosol radiative effects.

4. Results

4.1. Radiative Forcing

[19] Column aerosol optical properties and the surface albedo (ρ) at $\lambda = 550$ nm, and our best estimates of shortwave, diurnally averaged RF ± δRF are listed in Table 1, where the column-averaged values of $\omega_{o,550}$ and g_{550} are weighted by $\sigma_{ext,550}$. The values of δRF represent the 95% confidence intervals in RF and account for uncertainties in σ_{ext}, ω_o, g, and ρ as well as uncertainties in the flux calculated using the Fu-Liou RTM (section 3). The UW research aircraft obtained measurements of aerosol properties under many different aerosol loadings, with τ_{550} ranging from 0.16 to 1.13 (median is 0.34). The main driving force of τ_{550} in much of southern Africa during the dry season (Southern Hemisphere winter months) is biomass burning [*Eck et al.*, 2003]. There are relatively constant dust and industrial emission sources, but these play a smaller role compared to the impact of biomass burning emissions

[*Piketh et al.*, 1999; *Eck et al.*, 2003; *Gao et al.*, 2003; *Kirchstetter et al.*, 2003; *Sinha et al.*, 2003b]. Changes in the aerosol chemical composition affect $\omega_{o,550}$, which ranges from 0.81 to 0.93 (median is 0.87, consistent with the regional mean value of 0.85 ± 0.02 in the SAFARI-2000 analysis by *Leahy et al.* [2007]). For cases when $\omega_{o,550}$ was low, there was an increase in the carbonaceous mass to total mass ratio [*Gao et al.*, 2003; *Kirchstetter et al.*, 2003] that was mainly a result of an increase in biomass burning smoke density through a combination of changes in parcel back trajectories [*Magi and Hobbs*, 2003; *Stein et al.*, 2003], local and transported smoke [*Magi et al.*, 2003], and possibly changes in the fuel (i.e., the vegetation) being burned [*Korontzi et al.*, 2003; *Sinha et al.*, 2003a]. Aging of the southern African aerosol happens within hours after emission [*Magi and Hobbs*, 2003], so because the UW profiles were collected away from fire sources, aging played a smaller role in the changes in $\omega_{o,550}$ than the changes in smoke density discussed above. Advective transport plays a major role in the regional radiative impact of southern African biomass burning emissions [*Swap and Tyson*, 1999; *Stein et al.*, 2003], but this is better addressed by chemical transport models [*Sinha et al.*, 2004] or general circulation models [*Koch et al.*, 2007].

[20] RF_{toa} ranges from -1.5 to -14.4 W m^{-2}, with a median value of -7.5 W m^{-2}, while RF_{sfc} ranges from -10.5 to -81.3 W m^{-2} (median is -27.7 W m^{-2}). The range of RF_{sfc} is larger than the range of RF_{toa} because the increase in aerosol concentration enhances the amount of solar radiation attenuated before reaching the surface by both scattering more radiation away (higher τ) from the surface and absorbing more radiation (lower ω_o) before it reaches the surface. At the top of the atmosphere, however, more radiation (compared to an atmosphere without no aerosol loading) is scattered to space, but less radiation reaches the top of the atmosphere because of absorption in the atmosphere. Because of these competing effects of ω_o and τ, the values of RF_{toa} do not reveal potentially large differences in the aerosol optical properties. For example, RF_{toa} from the profiles on 14 August (1114 UTC) and 3 September (1012 UTC) are nearly the same at -7.1 ± 2.4 W m^{-2} and -7.0 ± 3.9 W m^{-2} (as are the values of g_{550} and ρ_{550}), but τ_{550} on 3 September is a factor of three higher while $\omega_{o,550}$ decreases by $\sim$7%. Referring to Figures 1a and 1b, these changes have strong effects on the RF at all levels. Simply assuming a single representative value of ω_o and adjusting τ may result in top of the atmosphere radiation budgets that are right for the wrong reasons and would most likely lead to incorrect surface (and atmospheric) radiation budgets. This could be an important point to consider in the development of satellite data products [e.g., *Ichoku et al.*, 2003; *Abdou et al.*, 2005; *Remer et al.*, 2005] and in understanding the output of chemical transport and general circulation models.

[21] The diurnally averaged radiative effects of the southern African aerosol on the atmosphere itself (RF_{atm}) are strongly warming since a great deal of solar radiation is absorbed, especially in cases when ω_o is low and τ is high (e.g., between 3 and 6 September). RF_{atm} is calculated as the difference between RF_{toa} and RF_{sfc} and ranges from 5.0 to 73.3 W m^{-2} (median is 19.5 W m^{-2}). Atmospheric absorption by the biomass burning aerosol in southern Africa therefore accounts for 47–92% of the surface cooling during the day. For comparison, the median value is 71% and is similar to the value of 67% presented by *Yu et al.* [2004] for biomass burning aerosol in South America and Africa. Depending on how representative the aerosol optical properties measured by the UW research aircraft are, the effect that the prolonged presence of a very absorbing aerosol layer has on the atmospheric structure in both tropical and subtropical southern Africa could be an interesting point for future scientific investigation.

[22] Uncertainties in the estimates of RF (δRF) are an important part of understanding the context of the results and are also listed in Table 1. We described in section 3 how we arrived at the final estimates of δRF, which, again, we interpret as the 95% confidence interval of the best estimates of RF. Values of δRF range from ± 2.3 to ± 12.4 W m^{-2}, with a median value of ± 3.6 W m^{-2}, implying that δRF tends toward the smaller values. The largest values of δRF are those associated with RF_{atm}, where the median value of δRF_{atm} is ± 4.5 W m^{-2}. This is due to the fact that δRF_{atm} is primarily determined by uncertainty in ω_o (section 3), and RF_{atm} (as well as RF_{toa} and RF_{sfc}) is very sensitive to ω_o (Figure 1b). The median values of δRF_{toa} and δRF_{sfc} are ± 2.8 W m^{-2} and ± 3.7 W m^{-2}, respectively. In general, the median percentage uncertainties in the estimates of RF_{toa}, RF_{atm}, and RF_{sfc} for southern African biomass burning aerosol are $\pm 43\%$, $\pm 22\%$, and $\pm 13\%$, respectively, keeping in mind the large differences in the magnitudes of RF_{toa}, RF_{atm}, and RF_{sfc}.

[23] The best method to assess the estimates of RF using UW research aircraft measurements is by comparison with independent measurements that are colocated in space and time. The ground-based Sun photometers in the Aerosol Robotic Network (AERONET) retrieved aerosol optical properties from measurements of sky radiance at a number of locations during SAFARI-2000 [*Eck et al.*, 2003]. *Leahy et al.* [2007] discussed five UW research aircraft vertical profiles which were within $\sim$19 km of the AERONET ground sites and obtained within $\sim$1 to 4 h of the AERONET retrieval times, minimizing the spatial and temporal changes in the aerosol between the times of the vertical profiles and the times of the AERONET retrievals [*Anderson et al.*, 2003b]. The retrieved submicron diameter particle size distributions using UW research aircraft data from SAFARI-2000 were similar to the submicron diameter particle size distributions from the AERONET retrieval, but the refractive indices did not agree [*Magi et al.*, 2007]. Thus, we can expect some differences in the estimates of RF using the UW retrieval and the AERONET retrieval.

[24] To compare the RF estimates in this study, we construct vertical profiles of aerosol properties using Version 2.0, Level 2.0 AERONET data products published online (http://aeronet.gsfc.nasa.gov/) for the five cases that are spatially and temporally colocated with the UW aircraft profiles [*Leahy et al.*, 2007]. We assume that τ retrieved from AERONET is uniformly distributed between the surface and the maximum altitude of the UW aircraft (3.8–4.8 km) for each case, and we assume that the column-averaged values of ω_o and g from AERONET apply to every layer between the surface and maximum altitude of the UW aircraft for each case. All other methods of con-

Table 2. Comparison of the Shortwave, Diurnally Averaged Radiative Forcing (RF) at the Top of the Atmosphere (RF_{toa}), Atmosphere (RF_{atm}), and Surface (RF_{sfc}) Estimated Using University of Washington (UW) and Aerosol Robotic Network (AERONET) Measurements Under Cloud-Free Conditions[a]

	UW	AERONET
	22 Aug 2000, 0816–1006 UTC	
RF_{toa}	−9.1 ± 2.7	−8.2 ± 2.8
RF_{atm}	14.9 ± 3.6	12.0 ± 3.4
RF_{sfc}	−24.1 ± 3.0	−20.2 ± 3.0
τ_{550}	0.36 ± 0.03	0.31 ± 0.02
$\omega_{o,550}$	0.91 ± 0.03	0.90 ± 0.03
g_{550}	0.57 ± 0.02	0.60 ± 0.04
	3 Sep 2000, 0831–0850 UTC	
RF_{toa}	−9.4 ± 4.7	−10.6 ± 4.4
RF_{atm}	52.2 ± 9.5	39.3 ± 5.0
RF_{sfc}	−61.6 ± 6.7	−49.9 ± 4.0
τ_{550}	0.80 ± 0.07	0.64 ± 0.02
$\omega_{o,550}$	0.84 ± 0.05	0.87 ± 0.03
g_{550}	0.54 ± 0.02	0.59 ± 0.04
	6 Sep 2000, 0746–0755 UTC	
RF_{toa}	−8.0 ± 4.0	−10.4 ± 4.4
RF_{atm}	72.4 ± 12.4	59.5 ± 6.9
RF_{sfc}	−80.4 ± 8.7	−69.9 ± 4.9
τ_{550}	1.13 ± 0.12	1.18 ± 0.02
$\omega_{o,550}$	0.83 ± 0.04	0.84 ± 0.03
g_{550}	0.59 ± 0.02	0.61 ± 0.04
	6 Sep 2000, 0917–0929 UTC	
RF_{toa}	−8.8 ± 4.8	−9.6 ± 4.9
RF_{atm}	72.5 ± 10.8	67.0 ± 7.8
RF_{sfc}	−81.3 ± 7.5	−76.6 ± 5.3
τ_{550}	1.12 ± 0.09	1.09 ± 0.02
$\omega_{o,550}$	0.83 ± 0.04	0.86 ± 0.03
g_{550}	0.58 ± 0.02	0.62 ± 0.04
	16 Sep 2000, 1052–1107 UTC	
RF_{toa}	−1.5 ± 3.2	0.5 ± 2.4
RF_{atm}	17.2 ± 3.7	13.6 ± 3.1
RF_{sfc}	−18.7 ± 2.8	−13.1 ± 2.6
τ_{550}	0.30 ± 0.03	0.30 ± 0.02
$\omega_{o,550}$	0.89 ± 0.04	0.86 ± 0.03
g_{550}	0.62 ± 0.02	0.67 ± 0.04

[a]Also listed are the aerosol optical properties at a wavelength of 550 nm from UW and AERONET. Notation is the same as in Table 1.

structing the vertical profiles used as input to the Fu-Liou RTM are identical to the methods used to convert the UW research aircraft data to RTM input (section 2 and Appendix A). The uncertainty analysis is also identical to the methods described in section 3, but we use $\delta\tau = \pm 0.02$, $\delta\omega_o = \pm 0.03$, and $\delta g = \pm 0.04$, following assessments by *Dubovik et al.* [2000, 2002], *Zhou et al.* [2005], and *Yu et al.* [2006]. The input to the Fu-Liou RTM is identical to the input derived from UW research aircraft measurements (section 2), except that we replace the shortwave aerosol optical properties in the lower atmosphere with shortwave aerosol optical properties retrieved from AERONET stations operating during SAFARI-2000.

[25] We estimate RF ± δRF using the profiles based on AERONET aerosol optical properties and list the results in Table 2 alongside the estimates of RF ± δRF based on UW research aircraft data. Of the 15 comparisons (RF_{toa}, RF_{atm}, and RF_{sfc} for each of the five cases), we say that the values of RF or the aerosol optical properties agree if the values are within the uncertainties listed in Table 2. Nine of the 15 comparisons of RF agree to within the estimated δRF. However, the agreement depends on the level in the atmosphere, with RF_{toa} having the best agreement (100%), RF_{atm} in agreement 60% of the time, and RF_{sfc} in agreement for 20% of the five cases.

[26] The agreement in RF depends on the agreement between the aerosol optical properties based on UW measurements and AERONET data products (listed in Table 2 for λ = 550 nm; usually, if there are differences in the aerosol optical properties at λ = 550 nm, then there are differences across the shortwave spectrum). On the basis of the results in Figure 1, we suggest that agreement mainly depends on the agreement between τ_{550} and $\omega_{o,550}$, and not as much on g_{550}, but that the effects of differences in aerosol optical properties on RF play out in complicated ways. Differences in τ_{550} affect the whole column, but the effect on RF becomes more apparent near the surface (for example, the case of 22 August with similar $\omega_{o,550}$ but different τ_{550}). Differences in $\omega_{o,550}$, on the other hand, strongly affect RF_{atm} and RF_{sfc}, especially when $\omega_{o,550}$ is low and τ_{550} is high (such as the three cases on 3 and 6 September). On 3 September in particular, the values of RF_{toa} from UW and AERONET agree to within the uncertainties, but there is poor agreement for RF_{atm} and RF_{sfc}. This can be traced to the 20% difference in τ_{550} from UW and from AERONET and the 4% difference in $\omega_{o,550}$. *Leahy et al.* [2007] speculated that a ~12% increase in AERONET τ_{550} between the 0709 UTC AERONET retrieval time and the 0831 UTC UW aircraft vertical profile time on that day was evidence of a changing air mass over the AERONET site and therefore offered an explanation of the discrepancy in $\omega_{o,550}$. Changes in τ_{550}, however, are not necessarily correlated with changes in intensive aerosol optical properties and thus the cause of the discrepancy remains unclear.

[27] Although most of the comparisons between UW and AERONET agree to within estimated uncertainties, there are discrepancies between aerosol optical properties that lead to much different estimates of RF_{atm} and RF_{sfc}. For the cases with similar aerosol optical properties, the agreement between estimates of RF based on column-averaged AERONET aerosol optical properties and RF based on vertically resolved profiles of aerosol optical properties from the UW research aircraft suggests that the use of AERONET data products will be very useful in models [*Chung et al.*, 2005; *Reddy et al.*, 2005a] and in measurement-based estimates of aerosol radiative effects [*Zhou et al.*, 2005; *Yu et al.*, 2006]. However, at least in southern Africa, we point out that there are discrepancies in the aerosol optical properties that are difficult to account for. Part of this may be due to assumptions in either the UW retrieval [*Magi et al.*, 2007] or in the AERONET retrieval [*Dubovik et al.*, 2000, 2002], but regional transport of biomass burning particles in southern Africa [*Swap and Tyson*, 1999; *Sinha et al.*, 2004] resulting in mesoscale variations [*Anderson et al.*, 2003b] may also have played a role in the differences. Regardless of the reasons, a proper validation of aerosol optical properties, and specifically ω_o, is critical to any estimate of RF, especially RF_{atm} and RF_{sfc}. Measurements of aerosol properties over AERONET sites [e.g., *Schmid et al.*, 2006] in

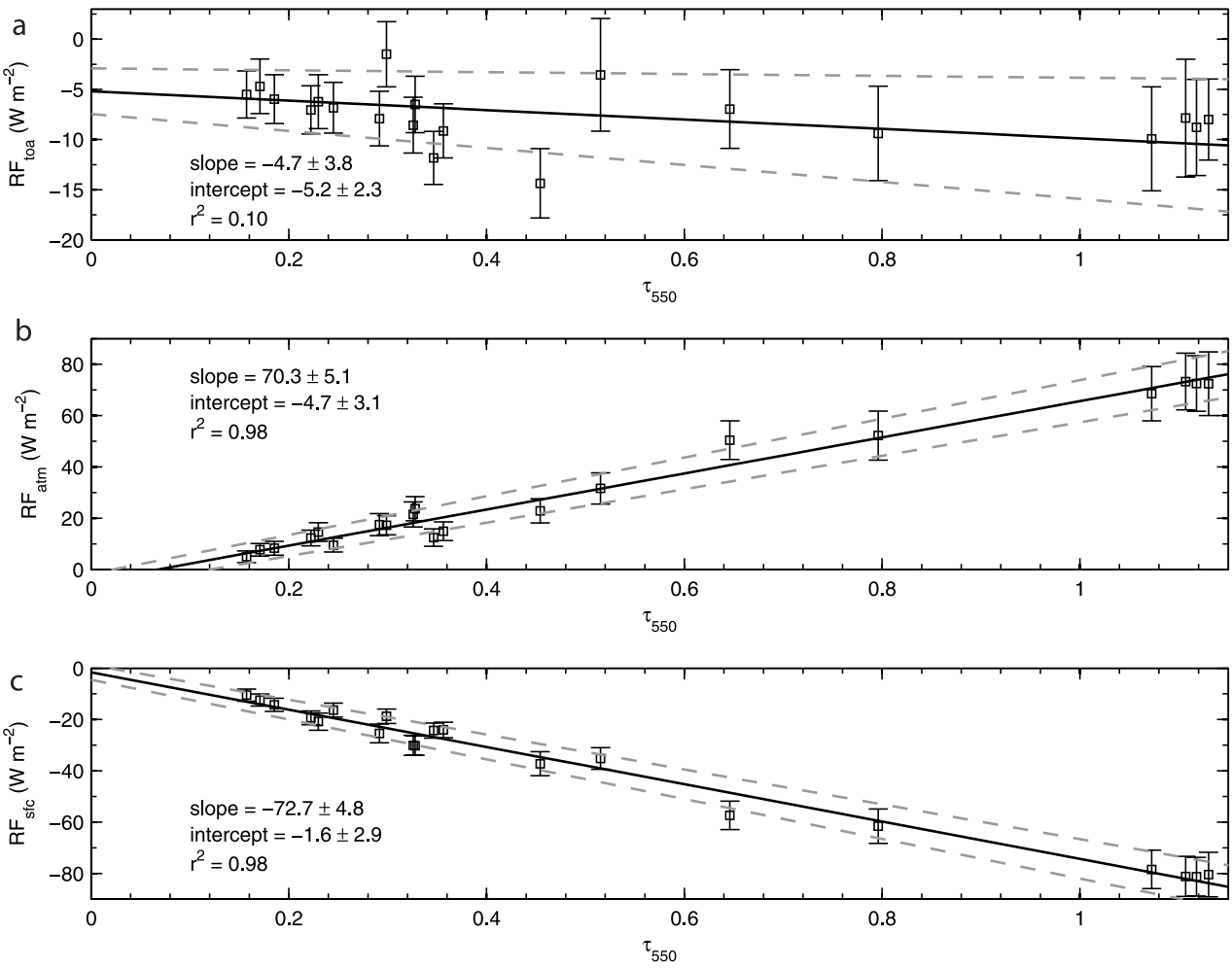

Figure 2. The cloud-free, diurnally averaged radiative forcing (RF) (a) at the top of the atmosphere (RF_{toa}), (b) atmosphere (RF_{atm}), and (c) surface (RF_{sfc}) shown as a function of the aerosol optical depth at a wavelength of 550 nm (τ_{550}). The vertical error bars are the 95% confidence limits in the estimates of RF. The dashed lines denote the 95% confidence interval about the statistical best fit (solid line).

particular would be extremely useful to the modeling and measurement communities.

4.2. Radiative Forcing Efficiency

[28] The aerosol radiative forcing efficiency (RFE) [*Anderson et al.*, 2005; *Yu et al.*, 2006] is a general way of relating RF, which can only be estimated using a model (section 2) or carefully selected measurements [e.g., *Bush and Valero*, 2002; *Jones and Christopher*, 2007], to τ_{550}, which is commonly measured [*Schmid et al.*, 2006] and retrieved [*Eck et al.*, 2003; *Ichoku et al.*, 2003; *Abdou et al.*, 2005; *Mishchenko et al.*, 2007]. Thus, RFE is defined as the radiative forcing per unit aerosol optical depth at $\lambda = 550$ nm (RF/τ_{550}) and is usually stated in units of W m^{-2} τ_{550}^{-1} to distinguish it from RF. One method to estimate RFE is the average instantaneous ratio of RF to τ_{550}, while another method is by fitting a line to the values of RF and τ_{550}. We use the second method since our sample size is only 20 data points and, as *Jones and Christopher* [2007] discuss, the regression method is not as sensitive to statistical variability and uncertainty in the data. RF is not necessarily linearly related to τ_{550} [e.g., *Anderson et al.*, 2005], but we show that in this study, RF can be approximated by a linear model for the aerosol over southern Africa. Similar to our discussions of RF, when we discuss RFE in this study, we are presenting the shortwave, diurnally averaged RFE of the aerosol over southern Africa during the biomass burning season in cloud-free conditions.

[29] In Figure 2, we show the relationship between the values of RF (RF_{toa}, RF_{atm}, and RF_{sfc}) and τ_{550} listed in Table 1 as well as listing the linear regression coefficients (slope and y-intercept). The linear models for RF shown in Figure 2 are

$$RF_{toa} = (-4.7 \pm 3.8)\tau_{550} - (5.2 \pm 2.3) \quad (1)$$

$$RF_{atm} = (70.3 \pm 5.1)\tau_{550} - (4.7 \pm 3.1) \quad (2)$$

$$RF_{sfc} = (-72.7 \pm 4.8)\tau_{550} - (1.6 \pm 2.9) \quad (3)$$

where the uncertainties in the equations are the 95% confidence intervals in the regression coefficients and are each based on N = 20 data points.

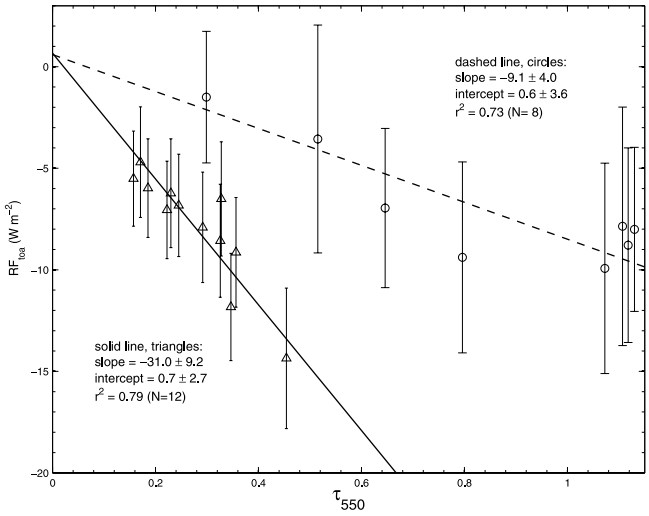

Figure 3. The cloud-free sky, diurnally averaged radiative forcing (RF) at the top of the atmosphere (RF_{toa}) as a function of aerosol optical depth at a wavelength of 550 nm (τ_{550}). The data are the same as Figure 2a, but here we show the statistically significant linear regressions to two subsets of the original N = 20 cases. We suggest that the linear relationship of RF_{toa} with τ_{550} itself depends on the magnitude of τ_{550}.

[30] In Figures 2b and 2c, most of the variance ($r^2 = 0.98$ for both cases) is explained by the linear fits of RF_{atm} and RF_{sfc} to τ_{550}, which suggests that the linear fits accurately model the data. However, the y-intercepts in Figures 2b and 2c are -4.7 W m^{-2} and -1.6 W m^{-2}, with the two standard deviation (95%) confidence intervals of the y-intercepts listed in Figures 2b and 2c. The zero y-intercept is contained within the 95% confidence interval of the y-intercept in Figure 2c (RF_{sfc}), but this is not the case in Figure 2b (RF_{atm}). Ideally, RF = 0 for $\tau_{550} = 0$ (i.e., when there is no aerosol), but we attribute the nonzero y-intercepts to either inaccuracies in the data or to nonlinearities in the relationship of RF and τ_{550} for $\tau_{550} < 0.16$ (data we do not have, see Table 1).

[31] For RF_{toa} in Figure 2a, the linear fit only explains 10% of the variance and therefore is not an accurate (or statistically significant) model. Using principle component (PC) analysis on the data [e.g., *Wilks*, 2006], we find that most of the total variance (96–99%) of RF_{atm} and RF_{sfc} is explained by the first PC, which is determined by the variations in τ_{550}. For RF_{toa}, however, 18% of the total variance is explained by the first PC while 82% is explained by a second PC. Physically, the second PC implies different mechanisms driving the relationship of RF_{toa} with τ_{550} (compared to RF_{atm} and RF_{sfc} with τ_{550}) and suggests that the linear relationship itself has a significant dependency. We parse the original 20 data points into two data sets that have the highest r^2 values. After we divide the data set, the linear fit improves from $r^2 = 0.10$ (N = 20) to $r^2 = 0.79$ (N = 12) and $r^2 = 0.73$ (N = 8). This dual model is now statistically significant at greater than the 95% confidence level, so we suggest that a better linear model for RFE_{toa} is one that is dependent on the magnitude of τ_{550}. For RF_{toa}, lower values of τ_{550} ($\tau_{550} < 0.5$) have one trend given by

$$RF_{toa} = (-31.0 \pm 9.2)\tau_{550} + (0.7 \pm 2.7) \quad (4)$$

and the higher values of τ_{550} ($\tau_{550} > 0.5$) have another trend given by

$$RF_{toa} = (-9.1 \pm 4.0)\tau_{550} + (0.6 \pm 3.6) \quad (5)$$

where the two linear regressions are shown in Figure 3, using a solid line with triangles (N = 12) for equation (4) and dashed line with circles (N = 8) for equation (5). This is the same data that is shown in Figure 2a (we do not apply this analysis to the data in Figures 2b and 2c since one linear model given by equations (2) and (3) explains a significant amount of the variance). The y-intercepts in Figure 3 are close to zero and contained within the 95% confidence interval error bars. Thus, where the first PC of RFE_{toa} is driven by variations in τ_{550}, the second PC is associated with the magnitude of τ_{550}.

[32] Physically, as shown in Table 1, the higher values of τ_{550} in southern Africa are typically associated with lower values of $\omega_{o,550}$ (see discussion in the beginning of section 4.1), and although this characteristic does not significantly affect RFE_{atm} and RFE_{sfc}, it does affect RFE_{toa}. RFE_{toa} for $\tau_{550} > 0.5$ (N = 8) is significantly different than RFE_{toa} for $\tau_{550} < 0.5$ (N = 12), as shown in Figure 3. The one "outlier" in this generalization is the case of the 16 September (1052 UTC) vertical profile where $\tau_{550} = 0.30$, but the data point is characteristic of the linear relationship of RFE_{toa} for $\tau_{550} > 0.5$ (equation (5)). We attribute this to the fact that $\rho_{550} = 0.19$ on that day (the surface was a bright dry lake bed called the Etosha Pan in Namibia) compared to the median value of $\rho_{550} = 0.08$ from the other data (Table 1). The case on 13 September (1116 UTC) also has a higher surface albedo than most of the other cases ($\rho_{550} = 0.18$), but because $\tau_{550} = 0.52$, the point does not deviate from the generalizations in equations (4) and (5). These two cases with high surface albedos are not very similar to the other data points, so we cannot conclusively say how representative the two cases are. However, we can point out that although the cases with high surface albedos may fit the overall trend for RFE_{toa} when $\tau_{550} > 0.5$, the physical reasons for this are different than the other data points where changes in the linear relationship are driven by changes in τ_{550} and $\omega_{o,550}$ (rather than ρ_{550} or even g_{550}).

[33] The estimates of RF based on independent measurements of aerosol optical properties from AERONET compared to within uncertainties the majority of the time in section 4.1, and now we compare the RFE derived in this study with values published in previous studies of the radiative effects of biomass burning particles over southern Africa. In a review study, *Yu et al.* [2006] reported values of RFE_{toa} and RFE_{sfc} for fine-mode aerosol (i.e., submicron diameter particles, which is similar to assumptions we make on the basis of limitations in the measurements discussed by *Magi et al.* [2007]) over southern Africa of -31.0 ± 9.2 W m^{-2} τ_{550}^{-1} and -87.2 ± 16.0 W m^{-2} τ_{550}^{-1}, respectively, based on AERONET climatologies compiled by *Zhou et al.* [2005], where the values are listed as mean and two standard deviations about the mean. *Yu et al.* [2006] suggest that

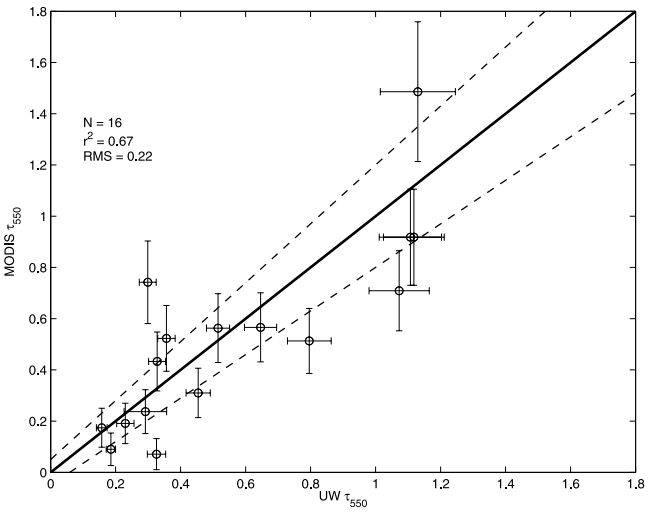

Figure 4. Comparison of N = 16 values of aerosol optical depth at a wavelength of 550 nm (τ_{550}) derived from MODIS satellite measurements and from the University of Washington (UW) measurements. The one-to-one line is drawn as a solid line, while the root-mean-squared (RMS) difference and linear correlation coefficient (r^2) between MODIS and UW τ_{550} are listed. Error bars are the estimated uncertainty in MODIS land-based τ_{550} and in UW τ_{550}. The dashed lines are the range about the one-to-one line determined by uncertainty in MODIS τ_{550} ($\pm 0.15 * \tau_{550} \pm 0.05$).

the natural variations (i.e., the two standard deviations) are generally larger than the uncertainties associated with the AERONET optical properties [e.g., *Dubovik et al.*, 2000, 2002]. *Zhou et al.* [2005] average the AERONET aerosol data products for each month at two AERONET locations (Mongu, Zambia and Skukuza, South Africa, see *Eck et al.* [2003]) and report annually averaged RFE_{toa} and RFE_{sfc} on the basis of monthly averaged aerosol optical properties, with $\tau_{550} = 0.18 \pm 0.12$ for southern Africa.

[34] In this study, using equation (3) with $\tau_{550} = 1$, RF_{sfc} is -74.3 ± 5.6 W m^{-2}, which is less than the average value given by *Yu et al.* [2006] but within the natural variability reported by AERONET. The linear regression for $\tau_{550} < 0.5$ (equation (4)) is more appropriate in the comparison since *Zhou et al.* [2005] use monthly averages of τ_{550}; from equation (4), $RF_{toa} = -30.3 \pm 9.6$ W m^{-2} at $\tau_{550} = 1$. This is very close to the annually averaged value reported by *Zhou et al.* [2005] and *Yu et al.* [2006]. We calculate the 95% confidence intervals using standard quadratures error propagation of the uncertainties in the regression coefficients in equations (3) and (4). The fact that RFE_{toa} and RFE_{sfc} derived using two different methodologies agreed within estimated variability and uncertainty offers some level of validation. However, the results in this study indicate that RFE_{toa} needs to be considered carefully to understand the relationship with the magnitude of τ_{550}, as summarized by equations (4)–(5).

4.3. Application

[35] We now apply the linear models in equations (2)–(5) (which we refer to as RFE) derived from UW measurements in section 4.2 to the available climatology of daily τ_{550} retrieved from the Moderate Resolution Imaging Spectroradiometer (MODIS) satellite [e.g., *Remer et al.*, 2005] using data published online (http://ladsweb.nascom.nasa.gov/) in MODIS Collection 5 (http://modis-atmos.gsfc.nasa.gov/products_C005update.html). We use MODIS daily 1° × 1° (latitude by longitude) τ_{550} from 1 March 2000 to 31 December 2006 for the southern African region defined as the land between 0–38°S latitude and 8–54°E longitude, excluding τ_{550} derived over ocean surfaces since RFE in this study is mainly over land surfaces. The daily latitude-longitude maps of τ_{550} from MODIS are often not complete because of cloud cover (e.g., over tropical southern Africa) or other problems preventing a proper retrieval. To derive RF under cloud-free skies, we estimate τ_{550} in the missing grid boxes as the average of the fifteen closest grid boxes in the unfilled land-based MODIS data set. The effect of this interpolation method is a 5–7% increase in the area-averaged daily τ_{550}, mainly since much of the missing data is in the regions of heavy biomass burning (and presumably high τ_{550}) in the cloud-laden tropics. The magnitudes of the cloud-free RF estimates presented here would be generally smaller when clouds are present [e.g., *Abel et al.*, 2005], except in the case of elevated aerosol advected over low clouds [*Keil and Haywood*, 2003].

[36] In Figure 4, we show the comparison of τ_{550} from UW research aircraft measurements (Table 1) to MODIS daily τ_{550} from the 1° × 1° pixel that contains the UW vertical profile. The linear correlation coefficient (r^2) of the regression between UW and MODIS τ_{550} is 0.67 (for N = 16 cases; four cases are excluded: three are on days with no MODIS data, and one is over an ocean surface) and the root-mean-squared (RMS) difference is 0.22 (40%). The agreement does not change significantly if we use the unfilled MODIS data ($r^2 = 0.63$, N = 14, RMS = 0.23). MODIS τ_{550} tends to be biased low compared to UW τ_{550} when UW $\tau_{550} > 0.6$ (for all but one case), while the bias is not consistent for $\tau_{550} < 0.6$. A larger sample size would be needed for a more conclusive comparison, but the low bias at high τ_{550} may be due to the comparison of a 1° × 1° pixel (~100 × 100 km) to a vertical profile encompassing a small fraction of this area (less than 10 × 10 km). Locally high τ_{550} sampled by the UW research aircraft would average out over the larger MODIS sample area. Referring to Collection 4 MODIS products and Version 1 AERONET products (both of which have significant updates that may affect the results), *Abdou et al.* [2005] showed that τ_{550} reported by MODIS and AERONET agreed to within about 0.15–0.19 (RMS), which is better than the agreement in this study. The uncertainty in MODIS τ_{550} is $\pm 0.05 \pm 0.15$ τ_{550} [*Remer et al.*, 2005], while uncertainties in UW τ_{550} range from 7 to 22% and are derived from uncertainties discussed by *Magi et al.* [2003, 2007]. Assuming the one-to-one comparison (solid line in Figure 4) is the desired result, MODIS and UW τ_{550} in Figure 4 agree to within the estimated uncertainties (error bars in Figure 4) for 50% of the cases considered. The statistically significant correlation ($r^2 = 0.67$), however, suggests that the overall trends in τ_{550} agree and provides some confidence in applying UW derived RFE to MODIS τ_{550}.

[37] We apply the linear models described in equations (2)–(5) to each 1° × 1° pixel in the (filled) maps of MODIS

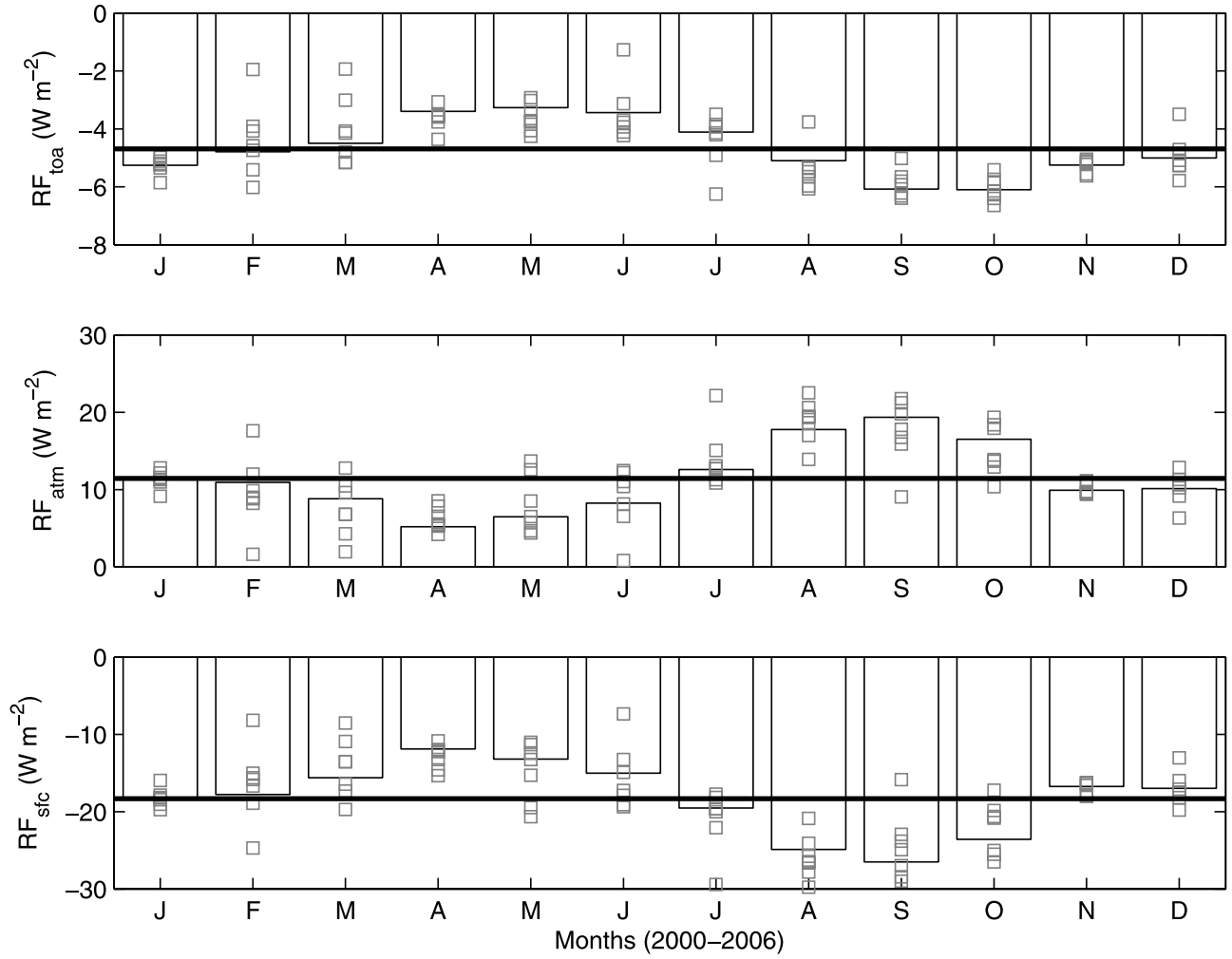

Figure 5. The monthly cloud-free sky, diurnally averaged radiative forcing (RF) at the top of the atmosphere (RF_{toa}), atmosphere (RF_{atm}), and surface (RF_{sfc}). We use MODIS daily aerosol optical depth at a wavelength of 550 nm (τ_{550}) from 1 March 2000 to 31 December 2006 together with relationships shown in Figures 2 and 3 to derive these values. The solid horizontal line is the annual RF. The vertical bars are the monthly RF averaged over 6 years, and the light gray squares are the individual monthly RF averaged over southern African land surfaces.

daily τ_{550} to derive maps of the daily RF from 1 March 2000 to 31 December 2006 over southern Africa. To derive RF_{toa}, we apply equation (4) when $\tau_{550} < 0.5$ and equation (5) when $\tau_{550} > 0.5$, while using equations (2) and (3) to derive RF_{atm} and RF_{sfc}, respectively. Because our linear model depends on the magnitude of the daily τ_{550}, we use the daily τ_{550} maps as opposed to monthly τ_{550} maps. We derive monthly RF maps from the daily RF maps, and average over the sample region to arrive at an area-averaged monthly RF for southern Africa (excluding ocean surfaces), as shown in Figure 5. The vertical bars in Figure 5 denote the mean values (of the 7 years of data) for each month and the grey points are monthly RF for each month from 2000 to 2006 (except January and February, which are from 2001 to 2006). The heavy horizontal line in Figure 5 is the annual RF (mean value of the height of the bars) for southern Africa. The interannual variability in the monthly RF (i.e., standard deviation in mean monthly RF) ranges from ±0.2 to 1.0 W m^{-2} (mean is ±0.6 W m^{-2}), ±0.8 to 3.8 W m^{-2} (mean is ±2.5 W m^{-2}), and ±0.9 to 3.9 W m^{-2} (mean is ±2.6 W m^{-2}) for RF_{toa}, RF_{atm}, and RF_{sfc}, respectively.

[38] To help understand how the variability in monthly RF is related to the uncertainty in monthly RF, we start by estimating the uncertainty in daily RF. To do this, we propagate the estimated uncertainties in MODIS land-based daily τ_{550} of $\pm 0.05 \pm 0.15\tau_{550}$ [*Remer et al.*, 2005] together with uncertainties in the regression coefficients listed in equations (2)–(5). The average (and two standard deviations) uncertainties in the daily RF_{toa}, RF_{atm}, and RF_{sfc} from 1 March 2000 to 31 December 2006 are 2.7 ± 0.6 W m^{-2}, 5.7 ± 1.5 W m^{-2}, 5.8 ± 1.6 W m^{-2}, respectively. Variability in the daily uncertainties over the sample period (daily for nearly 6 years) is relatively low, but is generally a maximum during times when τ_{550} is larger (i.e., during the biomass burning season). We suggest that the mean values of the daily uncertainties are a good estimate of 95% confidence interval in monthly and annual RF shown in Figure 5. Hence, we attribute uncertainties of ±2.7 W m^{-2}, ±5.7 W m^{-2},

and ±5.8 W m^{-2} to the monthly and annual RF_{toa}, RF_{atm}, and RF_{sfc}, respectively. These uncertainties are larger by factors of 2–4 than the variability in the monthly RF described above, suggesting that although there is most likely a trend in RF over the course of the year, the uncertainties in the magnitude of the monthly (or annual) RF exceed the natural variability.

[39] The uncertainties are each determined by three terms, but the dominant term is the uncertainty in MODIS τ_{550}, which accounts for an average of (65 ± 11)%, (91 ± 3)%, and (93 ± 2)% of the total daily uncertainties in RF_{toa}, RF_{atm}, and RF_{sfc}, respectively. The remaining uncertainty is due to uncertainties in the regression coefficients listed in equations (2)–(5). Improvements in the MODIS aerosol optical depth retrievals or in other satellite retrieval algorithms would be an important step in improving confidence in understanding aerosol effects on the radiative balance of the Earth.

[40] The validity of applying the linear models of RFE in equations (2)–(5) to a broad region of satellite derived τ_{550} is subject to basic assumptions. As discussed above and in Figure 4, although the correlation between UW and MODIS τ_{550} is good, the values only agree to within uncertainties for 50% of the cases. The assumption is therefore that the same relationships described by equations (2)–(5) could be derived using MODIS data. We do know that MODIS τ_{550} retrieval uses a value of $\omega_{o,550}$ that is within the estimated uncertainty of $\omega_{o,550}$ measured from the UW research aircraft [*Leahy et al.*, 2007], so we expect that the linear models we derive would be similar to those derived from MODIS τ_{550}. We also assume that the surface albedos over the region of interest do not vary significantly from the range listed in Table 1 and used to derive equations (2)–(5). The Kalahari and Namib desert regions in southwest southern Africa typically have higher surface albedos [e.g., *Moody et al.*, 2005] due to little or no vegetation [*Anyamba et al.*, 2003], but the largest τ_{550} is generally concentrated over the widespread woodland and grassland savannas [e.g., *Korontzi et al.*, 2003] with surface albedos consistent with those in Table 1. The dense rain forests of the Congo River basin have lower surface albedos, but a slightly darker surface should not affect the radiative calculations as much as a much brighter surface. Using the linear models in equations (2)–(5) then is justified since regions where the models would be most likely to fail generally have the smallest τ_{550} and therefore do not contribute greatly to the overall uncertainties.

[41] We also argue that the RFE derived from the aerosol measurements obtained from the UW research aircraft during SAFARI-2000 can be applied to the MODIS retrieved τ_{550} for the entire year. First, the UW measurements are an integrated characterization of the southern African aerosol and implicitly include any sort of background aerosol properties in addition to the more obvious biomass burning influence. A background aerosol might be similar to the cases with the lowest τ_{550} (when the profile is less impacted by biomass burning on that particular day). Thus, the RFE we derive implicitly accounts for more than biomass burning emissions. Second, the variability of aerosol optical properties over the year at the southern African AERONET sites in Mongu, Zambia, and in Skukuza, South Africa [*Zhou et al.*, 2005; *Yu et al.*, 2006] is captured in the range of the aerosol optical properties measured by the UW research aircraft (Table 1). Importantly, there are no prolonged peaks in the annual time series of τ_{550} from AERONET sites in Mongu or Skukuza except during the biomass burning season. A full analysis and source characterization is beyond the scope of this study, but we think this first-order analysis justifies the assumption that temporal variability of aerosol properties are captured by our estimates of RFE.

[42] There have been numerous other studies of the radiative impact of the southern African aerosol that addressed the regional impact [*Hansell et al.*, 2003; *Ichoku et al.*, 2003; *Myhre et al.*, 2003; *Abel et al.*, 2005], the difficulties in modeling aerosol advection [*Matichuk et al.*, 2007], the uncertainties in the aerosol properties [*Kinne et al.*, 2006], and even the global impact of the transported aerosol [*Koch et al.*, 2007]. In this study, we apply linear models of RFE to derive a more complete picture of RF based on daily variability in τ_{550} retrieved from MODIS satellite measurements. In lieu of a more rigorous verification of the applicability of this method with large-scale model output, we offer comparisons with other studies below as further evidence that the methods and the assumptions we make are justified. Although we address reasons for the differences, the different spatial and temporal scales in comparisons are compounded with the fact that aerosol loading varies as a function of biomass burning intensity (which fluctuates over a month), and that the specific aerosol properties depend on the proximity to source [*Sinha et al.*, 2003a; *Magi and Hobbs*, 2003] as well as regional variations in biomass burning intensity [*Eck et al.*, 2003].

[43] Using SAFARI-2000 measurements obtained over Namibia away from the major sources of biomass burning [*Keil and Haywood*, 2003; *Haywood et al.*, 2003a, 2003b; *Osborne et al.*, 2004], *Abel et al.* [2005] estimated that cloud-free RF_{toa} ranged from −3.2 to −21.6 W m^{-2} (mean of −7.6 W m^{-2}) and RF_{sfc} ranged from −7.8 to −57.6 W m^{-2} (mean of −18.1 W m^{-2}) over southern Africa during September, where they used the MODIS monthly average of September 2000–2003. The range of RF_{toa} roughly agrees with the range of −1.5 to −14.4 W m^{-2} (median of −7.5 W m^{-2}) presented in Table 1. This suggests that RF_{toa} does not vary dramatically over the course of a month and is consistent with both the limited range of RF_{toa} that can be derived using equations (4) and (5) as well as the small mean natural variability in monthly RF_{toa} of ±0.6 W m^{-2} derived above.

[44] Comparing our range of −10.5 to −81.3 W m^{-2} (median of −27.7 W m^{-2}) for RF_{sfc} to those reported by *Abel et al.* [2005], however, either suggests that variations in RF_{sfc} can be significant over a month due to varying aerosol properties or that there are differences in the aerosol properties used to simulate the southern African aerosol, or, more likely, both. Most likely, RF_{sfc} averaged over the month of September over a large region (that included ocean surfaces) is smaller than RF_{sfc} of the atmospheric columns profiled by the UW research aircraft on the particular days considered in this study. This may partly explain the discrepancy, but *Abel et al.* [2005] also used values of $\omega_{o,550}$ = 0.89 for most of southern Africa and $\omega_{o,550}$ = 0.84 for a smaller number of grid boxes containing a high number of active fires in September 2000 (i.e., near

the source). They point out that MODIS τ retrievals used in their study may underestimate τ when $\omega_{o,550}$ deviates from the regional value of $\omega_{o,550} = 0.90$ used by *Ichoku et al.* [2003], which is significantly larger than the regional value of 0.85 ± 0.02 suggested by *Leahy et al.* [2007]. However, there are important improvements in the MODIS τ retrievals as of 2006 (http://modis-atmos.gsfc.nasa.gov/products_C005update.html), which include changes in the treatment of the aerosol over biomass burning regions.

[45] If we use the monthly RF derived using MODIS τ_{550} (Collection 5) and relationships for RFE derived from UW research aircraft measurements (equations (2), (4), and (5)), we can provide a more direct comparison of the mean September 2000–2003 (hereafter, referred to as mean September) RF map with that presented by *Abel et al.* [2005]. We degraded the resolution of our plot to 4° × 5° as well to match the spatial resolution of the results presented by *Abel et al.* [2005], and the comparisons are strictly limited to land-based grid cells (see auxiliary material[1]). We estimate that mean September cloud-free RF_{toa} ranged from −1.1 to −8.9 W m^{-2} (mean and standard deviation of −6.4 ± 2.1 W m^{-2}, median of −7.5 W m^{-2}) and RF_{sfc} ranged from −5.7 to −60.6 W m^{-2} (−29.0 ± 14.5 W m^{-2}, median is −27.8 W m^{-2}) over southern Africa. Given the estimated uncertainty of ±2.7 W m^{-2} in RF_{toa} (discussed above), our mean September RF_{toa} of −6.4 W m^{-2} agrees with the value of −8.0 W m^{-2} derived by *Abel et al.* [2005]. Similarly, our mean September RF_{sfc} of −29.0 W m^{-2} also agrees with the value of −24.1 W m^{-2} by *Abel et al.* [2005] to within our estimated uncertainty of ±5.8 W m^{-2}. The maximum mean September RF_{sfc} in our study is −60.6 W m^{-2} and agrees with the maximum of −57.6 W m^{-2} by *Abel et al.* [2005], but there is a notable difference in the position of the maximum by about one grid cell (∼5°) to the northeast in our study. Regionally, the studies are in agreement, but over the northeastern part of southern Africa (roughly the Democratic Republic of the Congo and eastern Angola), RF_{sfc} does not agree to within our estimated uncertainties. We suggest that difference in the location of the maximum RF_{sfc} is mainly due to different aerosol optical properties (mainly ω_o) in that particular location. This may be an important point since the location of maximum RF_{sfc} is probably the area most impacted by burning emissions.

5. Conclusions

[46] We estimated the diurnally averaged, shortwave radiative forcing (RF) for 20 vertical profiles obtained by the University of Washington (UW) research aircraft in August and September 2000 during the Southern African Research Initiative or SAFARI-2000 [*Hobbs et al.*, 2003; *Swap et al.*, 2003]. We showed that the retrieval methodology given by *Magi et al.* [2007] combined with the methods presented in this study are a good method to transition from relatively common aircraft-based measurements of aerosol optical properties to radiative transfer model (RTM) input. The methods are also a good way to understand how the uncertainties in the aerosol optical properties translate to uncertainties in radiative forcing.

[47] Using the Fu-Liou RTM [*Liou et al.*, 1988; *Fu and Liou*, 1992], we compiled the best estimates of RF at the top of the atmosphere (RF_{toa}), by the atmosphere (RF_{atm}), and at the surface (RF_{sfc}). Estimates of RF_{toa}, RF_{atm}, and RF_{sfc} ranged from −1.5 to −14.4 W m^{-2} (median uncertainty of ±2.8 W m^{-2}), 5.0 to 73.3 W m^{-2} (median uncertainty of ±4.5 W m^{-2}), and −10.5 to −81.3 W m^{-2} (median uncertainty of ±3.7 W m^{-2}), respectively. We estimated the 95% confidence intervals of RF_{toa}, RF_{atm}, and RF_{sfc} (δRF_{toa}, δRF_{atm}, and δRF_{sfc}, respectively) through a series of sensitivity tests that account for uncertainties in the extinction coefficient (σ_{ext}), single scattering albedo (ω_o), asymmetry parameter (g), and surface albedo (ρ) and showed that uncertainty in ω_o accounts for most of the uncertainty in RF. A comparison of the RF estimated from UW research aircraft data with RF estimated using spatially and temporally colocated Aerosol Robotic Network (AERONET) station data [*Eck et al.*, 2003; *Leahy et al.*, 2007] for five cases showed that 60% of the comparisons (N = 15) agreed to within estimated uncertainties. The comparisons were best for RF_{toa} (100% agreement), and worst for RF_{sfc} (20% agreement), indicating that small differences in reported aerosol optical properties from the UW research aircraft [*Magi et al.*, 2003; *Schmid et al.*, 2003] and AERONET [*Eck et al.*, 2003; *Magi et al.*, 2007; *Leahy et al.*, 2007] will more strongly affect RF_{atm} and RF_{sfc} comparisons. Dedicated validation of AERONET data products by in situ measurements [e.g., *Schmid et al.*, 2006] could be invaluable in improving not only the understanding of southern African aerosol properties, but global aerosol properties.

[48] We derived robust relationships of RF with the aerosol optical depth at a wavelength of 550 nm (τ_{550}) using simple linear models. The linear relationship of RF with τ_{550} is also known as the radiative forcing efficiency (RFE) and has been discussed in many past studies as a possible way to relate a complicated calculation from radiative transfer (i.e., RF) to τ_{550} [e.g., *Anderson et al.*, 2005; *Jones and Christopher*, 2007]. RF is not necessarily always linearly related to τ_{550} [*Anderson et al.*, 2005], but we showed that for the southern African aerosol characteristics measured by the UW research aircraft during the biomass burning season, a linear model explains ∼98% of the variance for RFE_{atm} and RFE_{sfc} (equations (2) and (3)). The linear model for RFE_{toa}, however, suggests that RF_{toa} depends not only on variations in τ_{550}, but that the linear model itself is dependent on the magnitude of τ_{550}. Namely, we showed that there are two statistically significant trends for RFE_{toa} in equations (4) and (5), where one represents cases when $\tau_{550} < 0.5$ (equation (4)) and one represents cases when $\tau_{550} > 0.5$ (equation (5)). Using the linear models in equations (2)–(5) with $\tau_{550} = 1$, $RF_{toa} = -30.2 \pm 9.6$ W m^{-2} for $\tau_{550} < 0.5$ and $RF_{toa} = -8.5 \pm 5.4$ W m^{-2} for $\tau_{550} > 0.5$, while $RF_{atm} = 65.6 \pm 6.0$ W m^{-2} and $RF_{sfc} = -74.3 \pm 5.6$ W m^{-2}. These values agree to within uncertainties with values for southern Africa published by *Zhou et al.* [2005] and *Yu et al.* [2006].

[49] Finally, we applied the linear models shown in equations (2)–(5) to Moderate Resolution Imaging Spectroradiometer (MODIS) satellite [*Ichoku et al.*, 2003; *Remer*

[1] Auxiliary materials are available in the HTML. doi:10.1029/2007JD009258.

et al., 2005] derived values of daily τ_{550} (MODIS Collection 5 data products) for the southern African region from 1 March 2000 to 31 December 2006. Monthly RF_{toa} derived from MODIS daily τ_{550} and equations (4) and (5) only varies from -1.3 to -6.6 W m^{-2} over the course of the year. RF_{atm} and RF_{sfc}, on the other hand, vary from 0.8 to 22.5 W m^{-2} and -7.4 to -29.8 W m^{-2}, respectively. We suggest that the physical reason for the larger ranges in RF_{atm} and RF_{sfc} is that increases in the aerosol optical depth are primarily driven by increases in biomass burning emissions. This results in an increase in the relative contribution of carbonaceous matter to the overall aerosol composition and a coincident decrease in single scattering albedo. The radiative impact of the coincident changes are competing at the top of the atmosphere and complimentary in the atmosphere and at the surface. Hence, the variability in RF_{toa} will be smaller and mask changes in the aerosol optical properties in the atmosphere.

[50] Questions that arise from this study may be important in terms of large-scale modeling of the southern African aerosol. General circulation models [e.g., *Ginoux et al.*, 2006] and chemical transport models [e.g., *Kinne et al.*, 2006] typically underestimate the aerosol absorption over southern Africa, but often model the aerosol optical depths fairly well. This translates to a potential problem in modeling the chemical composition and might be traced to the disconnect between measurement studies and model development [*Ackerman et al.*, 2004; *Kahn et al.*, 2004]. Overall agreement in top of the atmosphere radiative budgets is not sufficient to suggest that regional aerosol properties in southern Africa are accurately modeled. Other regions of the world are also impacted by biomass burning or other combustion sources [*Bond et al.*, 2004], suggesting potentially similar issues as those we discuss for southern Africa. However, the biomass burning in South America [*Reid et al.*, 1998] occurs in atmospheres with higher relative humidity than southern Africa, which might temper the absorption to some degree. The biomass burning emissions in eastern Asia [*Doherty et al.*, 2005] and India [*Corrigan et al.*, 2006] interact with many different emission sources, precluding the natural simplifications that exist for southern Africa. In southern Africa, where the aerosol radiative effects are competing at the top of the atmosphere and complimentary at the surface, a better method to understand whether models capture aerosol properties reported by in situ measurements like in SAFARI-2000 would be to investigate atmospheric and surface radiation budgets.

Appendix A

[51] Uncertainties in the flux calculations associated with the approximations used in the computationally efficient Fu-Liou radiative transfer model (RTM) were assessed by *Liou et al.* [1988] and are less than ± 1 W m^{-2} in atmospheres with some absorption (i.e., $\omega_{o,550} < 1$) for the range of τ_{550} that we discuss in this study. We use the Henyey-Greenstein approximation to the scattering phase function [*Wiscombe and Grams*, 1976]. *Boucher* [1998] showed that for a purely scattering aerosol ($\omega_o = 1$), the difference in radiative forcing (RF) calculated using the Henyey-Greenstein approximation and RF calculated using the full Mie phase function can be significant at small and large solar zenith angles, especially for submicron diameter particles. The effect of the approximation for a range of real and imaginary refractive indices has not been published, but in this study, we account for this potentially additional uncertainty by doubling the uncertainty in the flux calculated by the Fu-Liou RTM to ± 2 W m^{-2} and include this as part of the final uncertainty estimates we discuss in section 3.

[52] We use the Fu-Liou RTM to calculate fluxes in cloud-free (clear sky) conditions at 100 levels from the surface to 500 hPa and 50 levels from 500 hPa to 25 hPa and calculate the diurnally averaged, shortwave RF using values of the solar zenith angles calculated every 30 min following equations in the work by *Liou* [2002]. The input to the model is mainly based on observations obtained from the University of Washington (UW) research aircraft during the SAFARI-2000 field campaign [*Magi et al.*, 2003; *Magi and Hobbs*, 2003; *Schmid et al.*, 2003]. Vertical profiles of temperatures (T) and water vapor mixing ratios are compiled using UW research aircraft measurements of T and relative humidity (RH) from the surface to $\sim$500 hPa and reanalysis data from the Fleet Naval Laboratory global model from $\sim$500 hPa to 25 hPa (http://www.arl.noaa.gov/ready/amet.html).

[53] Carbon dioxide (CO_2) and methane (CH_4) concentrations are set at 377 ppmv and 1770 ppbv, respectively [*Sinha et al.*, 2003b]. Nitrous oxide (N_2O) concentrations are based on *Thompson et al.* [2004] and set at 310 ppbv. We assume CO_2, CH_4, and N_2O are well mixed throughout the atmosphere. Vertical profiles of ozone (O_3) are constructed using UW research aircraft measurements of ozone [*Sinha et al.*, 2003b] and data from the Southern Hemisphere Additional Ozonesondes (SHADOZ) network that operated during SAFARI-2000 [*Thompson et al.*, 2002, 2003]. Generally, we use the UW research aircraft vertical profiles of O_3 from near the surface to $\sim$500 hPa and use data from the SHADOZ network for the remainder of the profile from $\sim$500 hPa to 25 hPa. We assume that the profiles of O_3 are not a source of uncertainty in the estimation of aerosol radiative forcing.

[54] We compile the vertical profiles of aerosol optical properties for the RTM using the SAFARI-2000 observations [*Magi et al.*, 2003] in the retrieval methodology described by *Magi et al.* [2007]. The vertical profiles by the UW research aircraft rarely exceeded 5 km above mean sea level (Table 1), so we use assumed properties for the unmeasured part of the atmospheric column. We used measurements of τ_λ at the top of the aircraft vertical profiles from the NASA Sun photometer [*Schmid et al.*, 2003] aboard the UW research aircraft [*Magi et al.*, 2003] to estimate the unmeasured aerosol loading above the maximum height of the vertical profile. Above that, upper atmospheric values of $\sigma_{ext,\lambda}$ are from satellite-derived upper atmospheric values of $\sigma_{ext,500}$ from a year 2003 climatology described by *Vanhellemont et al.* [2005] and we extrapolate $\sigma_{ext,500}$ across the shortwave spectrum using $\alpha_{ext} = 1$. We do not expect any significant variations in $\sigma_{ext,500}$ since no large volcanic eruptions occurred between 2000 and 2003. For upper atmospheric values of $\omega_{o,\lambda}$ and g_λ (for $\lambda = 200$–4000 nm), we use the climatology described by *Fenn et al.* [1985]. We use an exponential function to smoothly transition from the measured lower atmospheric aerosol optical properties (below 500 hPa) to the upper atmospheric (25 hPa

to 500 hPa) properties. Since the aircraft vertical profiles never quite reached the surface, we fill the part of the profile from the minimum altitude of the aircraft (Table 1) to the surface by simply assuming that the aerosol optical properties do not change from the bottom of the profile to the surface.

[55] The required spectral input to the Fu-Liou RTM are $\sigma_{ext,\lambda}$ (or τ_λ), $\omega_{o,\lambda}$, and g_λ for wavelengths in the entire shortwave spectrum, or λ = 200–4000 nm. We use the retrieval described by *Magi et al.* [2007] to compile self-consistent aerosol optical properties from λ = 354–1557 nm (the wavelength range of the instruments on the UW research aircraft). To extrapolate $\sigma_{ext,\lambda}$ to λ = 200–354 nm (1557–4000 nm), we use $\alpha_{ext,354-380}$ ($\alpha_{ext,1241-1557}$). We use an analogous approach to extrapolate $\sigma_{sca,\lambda}$ and τ_λ. We calculate $\omega_{o,\lambda}$ ($\sigma_{sca,\lambda}/\sigma_{ext,\lambda}$) using the values of $\sigma_{ext,\lambda}$ and $\sigma_{sca,\lambda}$ for the shortwave spectrum and extrapolate g_λ to $\lambda <$ 354 nm ($\lambda >$ 1557 nm) using a linear regression to values of g_λ at 354, 380, and 449 nm (1019, 1241, and 1557 nm).

[56] After we have the shortwave aerosol optical properties at discrete wavelengths from the surface to 25 hPa, we then calculate a weighted average value of the properties over the fifteen shortwave wavelength bands of the Fu-Liou RTM (see Table 2 for a detailed listing of the Fu-Liou wavelength bands). This so-called "band averaging" is necessary to account for variations in the aerosol properties and in the solar irradiance spectrum over a specific wavelength band. The band-averaged values of σ_{ext}, ω_o, and g ($\sigma_{ext,\lambda_1-\lambda_2}$, $\omega_{o,\lambda_1-\lambda_2}$, and $g_{\lambda_1-\lambda_2}$, respectively, where λ_1 and λ_2 are the edges of the wavelength band) are calculated as

$$\sigma_{ext,\lambda_1-\lambda_2} = \frac{\int_{\lambda_1}^{\lambda_2} \sigma_{ext,\lambda} S_\lambda d\lambda}{\int_{\lambda_1}^{\lambda_2} S_\lambda d\lambda} \tag{A1}$$

$$\omega_{o,\lambda_1-\lambda_2} = \frac{\int_{\lambda_1}^{\lambda_2} \omega_{o,\lambda}\sigma_{ext,\lambda} S_\lambda d\lambda}{\int_{\lambda_1}^{\lambda_2} \sigma_{ext,\lambda} S_\lambda d\lambda} \tag{A2}$$

$$g_{\lambda_1-\lambda_2} = \frac{\int_{\lambda_1}^{\lambda_2} g_\lambda \omega_{o,\lambda}\sigma_{ext,\lambda} S_\lambda d\lambda}{\int_{\lambda_1}^{\lambda_2} \omega_{o,\lambda}\sigma_{ext,\lambda} S_\lambda d\lambda} \tag{A3}$$

where S_λ is the solar irradiance spectrum at the top of the atmosphere from *Thekaekara* [1973]. These calculations are done for every Fu-Liou RTM band and used as the final input to the Fu-Liou RTM.

[57] Except for θ_o, we do not attempt to model diurnal variations in the aerosol optical properties. Biomass burning has a diurnal cycle that is stronger in countries such as Zambia (i.e., tropical southern Africa) and weaker in the region around northern South Africa and this results in diurnal variations in the extensive aerosol optical properties [*Eck et al.*, 2003]. *Eck et al.* [2003] show that the daily range in τ_λ can be as much as 25% in the tropical regions, but falls off to 5–10% in countries further to the south, and that in most cases fire activity peaks in the afternoon (local time is UTC + 2, referring to the times of the vertical profiles listed in Table 1). There are no direct measurements of the diurnal variability of $\omega_{o,\lambda}$ and g_λ. On the order of a single day, changes in smoke concentration due to increasing or decreasing local fire activity should primarily affect τ_λ or $\sigma_{ext,\lambda}$ (properties dependent on the particle concentration) For periods longer than a day, however, $\omega_{o,\lambda}$ and g_λ will certainly change depending on the interaction between synoptic-scale meteorology [*Garstang et al.*, 1996; *Stein et al.*, 2003] and biomass burning emission location and intensity. We assume that a single vertical profile of aerosol optical properties is an adequate model of the diurnally averaged vertical profile.

[58] **Acknowledgments.** We thank the late Peter Hobbs for his support during the research phase of this project. Valuable discussions with Dean Hegg, Tad Anderson, Tom Ackerman, and Steven Abel, as well as comments by anonymous reviewers helped improve this project. We thank Brent Holben and Stuart Piketh for their efforts in establishing and maintaining the Mongu, Sua Pan, and Skukuza AERONET (http://aeronet.gsfc.nasa.gov) sites in southern Africa. We also thank members of the NASA satellite community for developing and maintaining the Giovanni (http://disc.sci.gsfc.nasa.gov/giovanni/) and the LAADS (http://ladsweb.nascom.nasa.gov/) online data archives. B.M. was supported by NSF grant 0314453. Q. F. was in part supported by NASA grant NNG04GM23G.

References

Abel, S. J., E. J. Highwood, J. M. Haywood, and M. A. Stringer (2005), The direct radiative effects of biomass burning aerosols over southern Africa, *Atmos. Chem. Phys.*, *5*, 1999–2018.

Abdou, W. A., D. J. Diner, J. V. Martonchik, C. J. Bruegge, R. A. Kahn, B. J. Gaitley, K. A. Crean, L. A. Remer, and B. Holben (2005), Comparison of coincident Multiangle Imaging Spectroradiometer and Moderate Resolution Imaging Spectroradiometer aerosol optical depths over land and ocean scenes containing Aerosol Robotic Network sites, *J. Geophys. Res.*, *110*, D10S07, doi:10.1029/2004JD004693.

Ackerman, T. P., and O. B. Toon (1981), Absorption of visible radiation in atmosphere containing mixtures of absorbing and nonabsorbing particles, *Appl. Opt.*, *20*(20), 3661–3668.

Ackerman, T. P., A. J. Braverman, D. J. Diner, T. L. Anderson, R. A. Kahn, J. V. Martonchik, J. E. Penner, P. J. Rasch, B. A. Wielicki, and B. Yu (2004), Integrating and interpreting aerosol observations and models within the PARAGON framework, *Bull. Am. Meteorol. Soc.*, *85*, 1523–1533.

Anderson, T. L., R. J. Charlson, S. E. Schwartz, R. Knutti, O. Boucher, H. Rodhe, and J. Heintzenberg (2003a), Climate forcing by aerosols—A hazy picture, *Science*, *300*, 1103–1104.

Anderson, T. L., R. J. Charlson, D. M. Winker, J. A. Ogren, and K. Holmen (2003b), Mesoscale variations of tropospheric aerosols, *J. Atmos. Sci.*, *60*, 119–136.

Anderson, T. L., et al. (2005), An "A-Train" strategy for quantifying direct climate forcing by anthropogenic aerosols, *Bull. Am. Meteorol. Soc.*, *85*, 1795–1809.

Andreae, M. O., C. D. Jones, and P. M. Cox (2005), Strong present-day aerosol cooling implies a hot future, *Nature*, *435*, 1187–1190.

Anyamba, A., C. O. Justice, C. J. Tucker, and R. Mahoney (2003), Seasonal to interannual variability of vegetation and fires at SAFARI 2000 sites inferred from advanced very high resolution radiometer times series data, *J. Geophys. Res.*, *108*(D13), 8507, doi:10.1029/2002JD002464.

Bergstrom, R. W., P. Pilewskie, B. Schmid, and P. B. Russell (2003), Estimates of the spectral aerosol single scattering albedo and aerosol radiative effects during SAFARI 2000, *J. Geophys. Res.*, *108*(D13), 8474, doi:10.1029/2002JD002435.

Bond, T. C., and R. W. Bergstrom (2006), Light absorption by carbonaceous particles: An investigative review, *Aerosol Sci. Technol.*, *40*, 27–67.

Bond, T. C., D. G. Streets, K. F. Yarber, S. M. Nelson, J. Woo, and Z. Klimont (2004), A technology-based global inventory of black and organic carbon emissions from combustion, *J. Geophys. Res.*, *109*, D14203, doi:10.1029/2003JD003697.

Boucher, O. (1998), On aerosol direct shortwave forcing and the Henyey-Greenstein phase function, *J. Atmos. Sci.*, *55*, 128–134.

Bush, B. C., and F. P. J. Valero (2002), Spectral aerosol radiative forcing at the surface during the Indian Ocean Experiment (INDOEX), *J. Geophys. Res.*, *107*(D19), 8003, doi:10.1029/2000JD000020.

Christopher, S. A., X. Li, R. M. Welch, J. S. Reid, P. V. Hobbs, T. F. Eck, and B. Holben (2000), Estimation of surface and top-of-atmosphere shortwave irradiance in biomass-burning regions during SCAR-B, *J. Appl. Meteorol.*, *39*, 1742–1753.

Chung, C. E., V. Ramanathan, D. Kim, and I. A. Podgorny (2005), Global anthropogenic aerosol direct forcing derived from satellite and ground-based observations, *J. Geophys. Res.*, *110*, D24207, doi:10.1029/2005JD006356.

Chung, S. H., and J. H. Seinfeld (2005), Climate response of direct radiative forcing of anthropogenic black carbon, *J. Geophys. Res.*, *110*, D11102, doi:10.1029/2004JD005441.

Chylek, P., V. Srivastava, R. G. Pinnick, and R. T. Wang (1988), Scattering of electromagnetic waves by composite spherical particles: Experiment and effective medium approximations, *Appl. Opt.*, *27*, 2396–2404.

Clarke, A. D., et al. (2002), INDOEX aerosol: A comparison and summary of chemical microphysical, and optical properties observed from land, ship, and aircraft, *J. Geophys. Res.*, *107*(D19), 8033, doi:10.1029/2001JD000572.

Corrigan, C. E., V. Ramanathan, and J. J. Schauer (2006), Impact of monsoon transition on the physical and optical properties of aerosols, *J. Geophys. Res.*, *111*, D18208, doi:10.1029/2005JD006370.

Cosijn, C., and P. D. Tyson (1996), Stable discontinuities in the atmosphere over South Africa, *S. Afr. J. Sci.*, *92*, 381–386.

d'Almeida, G. A., P. Koepke, and E. P. Shettle (Eds.) (1991), *Atmospheric Aerosols: Global Climatology and Radiative Characteristics*, 561 pp., A. Deepak, Hampton, Va.

Delworth, T. L., V. Ramaswamy, and G. L. Stenchikov (2005), The impacts of aerosols on simulated ocean temperature and heat content in the 20th century, *Geophys. Res. Lett.*, *32*, L24709, doi:10.1029/2005GL024457.

Doherty, S., P. K. Quinn, A. Jefferson, C. M. Carrico, T. L. Anderson, and D. Hegg (2005), A comparison and summary of aerosol optical properties as observed in situ from aircraft, ship, and land during ACE-Asia, *J. Geophys. Res.*, *110*, D04201, doi:10.1029/2004JD004964.

Dubovik, O., A. Smirnov, B. N. Holben, M. D. King, Y. J. Kaufman, T. F. Eck, and I. Slutsker (2000), Accuracy assessments of aerosol optical properties retrieved from Aerosol Robotic Network (AERONET) Sun and sky radiance measurements, *J. Geophys. Res.*, *105*(D8), 9791–9806.

Dubovik, O., B. Holben, T. F. Eck, A. Smirnov, Y. J. Kaufman, M. D. King, D. Tanre, and I. Slutsker (2002), Variability of absorption and optical properties of key aerosol types observed in worldwide locations, *J. Atmos. Sci.*, *59*, 590–608.

Eck, T. F., et al. (2003), Variability of biomass burning aerosol optical characteristics in southern Africa during the SAFARI 2000 dry season campaign and a comparison of single scattering albedo estimates from radiometric measurements, *J. Geophys. Res.*, *108*(D13), 8477, doi:10.1029/2002JD002321.

Fenn, R. W., S. A. Clough, W. O. Gallery, R. E. Good, F. X. Kneizys, J. D. Mill, L. S. Rothman, E. P. Shettle, and F. E. Volz (1985), Optical and infrared properties of the atmosphere, in *Handbook of Geophysics and the Space Environment*, edited by A. S. Jursa, pp. 18-1–18-71, Air Force Geophys. Lab., Hanscom Air Force Base, Bedford, Mass.

Fu, Q., and K. N. Liou (1992), On the correlated k-distribution method for radiative transfer in nonhomogeneous atmospheres, *J. Atmos. Sci.*, *49*, 2139–2156.

Gao, S., D. A. Hegg, P. V. Hobbs, T. W. Kirchstetter, B. I. Magi, and M. Sadilek (2003), Water-soluble organic components in aerosols associated with savanna fires in southern Africa: Identification, evolution, and distribution, *J. Geophys. Res.*, *108*(D13), 8491, doi:10.1029/2002JD002324.

Garstang, M., P. D. Tyson, R. Swap, M. Edwards, P. Kallberg, and J. A. Lindesay (1996), Horizontal and vertical transport of air over southern Africa, *J. Geophys. Res.*, *101*(D19), 23,721–23,736.

Gatebe, C. K., M. D. King, S. Platnick, G. T. Arnold, E. F. Vermote, and B. Schmid (2003), Airborne spectral measurements of surface-atmosphere anisotropy for several surfaces and ecosystems over southern Africa, *J. Geophys. Res.*, *108*(D13), 8489, doi:10.1029/2002JD002397.

Ginoux, P., L. W. Horowitz, V. Ramaswamy, I. V. Geogdzhayev, B. N. Holben, G. Stenchikov, and X. Tie (2006), Evaluation of aerosol distribution and optical depth in the Geophysical Fluid Dynamics Laboratory coupled model CM2.1 for present climate, *J. Geophys. Res.*, *111*, D22210, doi:10.1029/2005JD006707.

Hansell, R. A., S. Tsay, Q. Ji, K. N. Liou, and S. Ou (2003), Surface aerosol radiative forcing derived from collocated ground-based radiometric observations during PRIDE, SAFARI, and ACE-Asia, *Appl. Opt.*, *42*(27), 5533–5544.

Hartley, W. S., and P. V. Hobbs (2001), An aerosol model and aerosol-induced changes in the clear-sky albedo off the east coast of the United States, *J. Geophys. Res.*, *106*(D9), 9733–9748.

Haywood, J. M., S. R. Osborne, P. N. Francis, A. Keil, P. Formenti, M. O. Andreae, and P. H. Kaye (2003a), The mean physical and optical properties of regional haze dominated biomass burning aerosol measured from the C-130 aircraft during SAFARI 2000, *J. Geophys. Res.*, *108*(D13), 8473, doi:10.1029/2002JD002226.

Haywood, J., P. Francis, O. Dubovik, M. Glew, and B. Holben (2003b), Comparison of aerosol size distributions, radiative properties, and optical depths determined by aircraft observations and Sun photometers during SAFARI 2000, *J. Geophys. Res.*, *108*(D13), 8471, doi:10.1029/2002JD002250.

Hess, M., P. Koepke, and I. Schult (1998), Optical properties of aerosols and clouds: The software package OPAC, *Bull. Am. Meteorol. Soc.*, *79*(5), 831–844.

Hobbs, P. V., P. Sinha, R. J. Yokelson, I. T. Bertschi, D. R. Blake, S. Gao, T. W. Kirchstetter, T. Novakov, and P. Pilewskie (2003), Evolution of gases and particles from a savanna fire in South Africa, *J. Geophys. Res.*, *108*(D13), 8485, doi:10.1029/2002JD002352.

Ichoku, C., L. A. Remer, Y. J. Kaufman, R. Levy, D. A. Chu, D. Tanre, and B. N. Holben (2003), MODIS observation of aerosols and estimation of aerosol radiative forcing over southern Africa during SAFARI 2000, *J. Geophys. Res.*, *108*(D13), 8499, doi:10.1029/2002JD002366.

Jacobson, M. Z. (2001), Global direct radiative forcing due to multicomponent anthropogenic and natural aerosols, *J. Geophys. Res.*, *106*(D2), 1551–1568.

Jones, T. A., and S. A. Christopher (2007), Statistical variability of top of atmosphere cloud-free shortwave aerosol radiative effect, *Atmos. Chem. Phys.*, *7*, 2937–2948.

Kahn, R. A., J. A. Ogren, T. P. Ackerman, J. Boesenberg, R. J. Charlson, D. J. Diner, B. N. Holben, R. T. Menzies, M. A. Miller, and J. H. Seinfeld (2004), Aerosol data sources and their roles within PARAGON, *Bull. Am. Meteorol. Soc.*, *85*, 1511–1522.

Keil, A., and J. M. Haywood (2003), Solar radiative forcing by biomass burning aerosol particles during SAFARI 2000: A case study based on measured aerosol and cloud properties, *J. Geophys. Res.*, *108*(D13), 8467, doi:10.1029/2002JD002315.

Kinne, S., et al. (2006), An AeroCom initial assessment—Optical properties in aerosol component modules of global models, *Atmos. Chem. Phys.*, *6*, 1815–1834.

Kirchstetter, T. W., T. Novakov, P. V. Hobbs, and B. Magi (2003), Airborne measurements of carbonaceous aerosols in southern Africa during the dry biomass burning season, *J. Geophys. Res.*, *108*(D13), 8476, doi:10.1029/2002JD002171.

Koch, D., T. C. Bond, D. Streets, N. Unger, and G. R. van der Werf (2007), Global impacts of aerosols from particular source regions and sectors, *J. Geophys. Res.*, *112*, D02205, doi:10.1029/2005JD007024.

Korontzi, S., D. E. Ward, R. A. Susott, R. J. Yokelson, C. O. Justice, P. V. Hobbs, E. A. H. Smithwick, and W. M. Hao (2003), Seasonal variation and ecosystem dependence of emission factors for selected trace gases and $PM_{2.5}$ for southern African savanna fires, *J. Geophys. Res.*, *108*(D24), 4758, doi:10.1029/2003JD003730.

Leahy, L. V., T. L. Anderson, T. F. Eck, and R. W. Bergstrom (2007), A synthesis of single scattering albedo of biomass burning aerosol over southern Africa during SAFARI 2000, *Geophys. Res. Lett.*, *34*, L12814, doi:10.1029/2007GL029697.

Li, J., M. Posfai, P. V. Hobbs, and P. R. Buseck (2003), Individual aerosol particles from biomass burning in southern Africa: 2. Compositions and aging of inorganic particles, *J. Geophys. Res.*, *108*(D13), 8484, doi:10.1029/2002JD002310.

Liao, H., and J. H. Seinfeld (1998), Radiative forcing by mineral dust aerosols: Sensitivity to key variables, *J. Geophys. Res.*, *103*(D24), 31,637–31,645.

Liou, K. N. (2002), *An Introduction to Atmospheric Radiation*, 2nd ed., 583 pp., Academic, Boston, Mass.

Liou, K. N., Q. Fu, and T. P. Ackerman (1988), A simple formulation of the delta-four-stream approximation for radiative transfer parameterization, *J. Atmos. Sci.*, *45*(13), 1940–1947.

Magi, B. I. (2006), Optical properties and radiative forcing of southern African biomass burning aerosol, Ph.D. thesis, 180 pp., Univ. of Wash., Seattle.

Magi, B. I., and P. V. Hobbs (2003), Effects of humidity on aerosols in southern Africa during the biomass burning season, *J. Geophys. Res.*, *108*(D13), 8495, doi:10.1029/2002JD002144.

Magi, B. I., P. V. Hobbs, B. Schmid, and J. Redemann (2003), Vertical profiles of light scattering, light absorption, and single scattering albedo during the dry, biomass burning season in southern Africa and comparisons of in situ and remote sensing measurements of aerosol optical depths, *J. Geophys. Res.*, *108*(D13), 8504, doi:10.1029/2002JD002361.

Magi, B. I., P. V. Hobbs, T. W. Kirchstetter, T. Novakov, D. A. Hegg, S. Gao, J. Redemann, and B. Schmid (2005), Aerosol properties and

chemical apportionment of aerosol optical depth at locations off the United States East Coast in July and August 2001, *J. Atmos. Sci.*, *62*(4), 919–933.

Magi, B. I., Q. Fu, and J. Redemann (2007), A methodology to retrieve self-consistent aerosol optical properties using common aircraft measurements, *J. Geophys. Res.*, *112*, D24S12, doi:10.1029/2006JD008312.

Matichuk, R. I., P. R. Colarco, J. A. Smith, and O. B. Toon (2007), Modeling the transport and optical properties of smoke aerosols from African savanna fires during the Southern African Regional Science Initiative campaign (SAFARI 2000), *J. Geophys. Res.*, *112*, D08203, doi:10.1029/2006JD007528.

McComiskey, A., S. E. Schwartz, B. Schmid, H. Guan, P. Ricchiazzi, E. R. Lewis, and J. A. Ogren (2008), Direct aerosol forcing: Calculation from observables and sensitivities to inputs, *J. Geophys. Res*, doi:10.1029/2007JD009170, in press.

McGill, M. J., D. L. Hlavka, W. D. Hart, E. J. Welton, and J. R. Campbell (2003), Airborne lidar measurements of aerosol optical properties during SAFARI-2000, *J. Geophys. Res.*, *108*(D13), 8493, doi:10.1029/2002JD002370.

Mishchenko, M. I., I. V. Geogdzhayev, W. B. Rossow, B. Cairns, B. E. Carlson, A. A. Lacis, L. Liu, and L. D. Travis (2007), Long-term satellite record reveals likely recent aerosol trend, *Science*, *315*, 1543.

Moody, E. G., M. D. King, S. Platnick, C. B. Schaaf, and F. Gao (2005), Spatially complete global spectral surface albedos: Value-added datasets derived from Terra MODIS land products, *IEEE Trans. Geosci. Remote Sens.*, *43*(1), 144–158.

Myhre, G., T. K. Berntsen, J. M. Haywood, J. K. Sundet, B. N. Holben, M. Johnsrud, and F. Stordal (2003), Modeling the solar radiative impact of aerosols from biomass burning during the Southern African Regional Science Initiative (SAFARI-2000) experiment, *J. Geophys. Res.*, *108*(D13), 8501, doi:10.1029/2002JD002313.

Osborne, S. R., J. M. Haywood, P. N. Francis, and O. Dubovik (2004), Short-wave radiative effects of biomass burning aerosol during SAFARI-2000, *Q. J. R. Meteorol. Soc.*, *130*, 1423–1447.

Piketh, S. J., H. J. Annegarn, and P. D. Tyson (1999), Lower tropospheric aerosol loadings over South Africa: The relative contribution of aeolian dust, industrial emissions, and biomass burning, *J. Geophys. Res.*, *104*(D1), 1597–1607.

Pilewskie, P., J. Pommier, R. Bergstrom, W. Gore, S. Howard, M. Rabbette, B. Schmid, P. V. Hobbs, and S. C. Tsay (2003), Solar spectral radiative forcing during the Southern African Regional Science Initiative, *J. Geophys. Res.*, *108*(D13), 8486, doi:10.1029/2002JD002411.

Posfai, M., R. Simonics, J. Li, P. V. Hobbs, and P. R. Buseck (2003), Individual aerosol particles from biomass burning in southern Africa: 1. Compositions and size distributions of carbonaceous particles, *J. Geophys. Res.*, *108*(D13), 8483, doi:10.1029/2002JD002291.

Quinn, P. K., and T. S. Bates (2005), Regional aerosol properties: Comparisons from ACE 1, ACE 2, Aerosols99, INDOEX, ACE Asia, TARFOX, and NEAQS, *J. Geophys. Res.*, *110*, D14202, doi:10.1029/2004JD004755.

Ramaswamy, V., O. Boucher, J. Haigh, D. Hauglustaine, J. M. Haywood, G. Myhre, T. Nakajima, G. Y. Shi, and S. Solomon (2001), Radiative forcing of climate change, in *Climate Change 2001: The Scientific Basis—Contribution of Working Group I to the Third Assessment Report of the Intergovernmental Panel on Climate Change*, edited by J. T. Houghton, et al., pp. 349–416, Cambridge Univ. Press, New York.

Reddy, M. S., O. Boucher, N. Bellouin, M. Schulz, Y. Balkanski, J. L. Dufresne, and M. Pham (2005a), Estimates of global multicomponent aerosol optical depth and direct radiative perturbation in the Laboratoire de Meteorologie-Dynamique general circulation model, *J. Geophys. Res.*, *110*, D10S16, doi:10.1029/2004JD004757.

Reddy, M. S., O. Boucher, Y. Balkanski, and M. Schulz (2005b), Aerosol optical depths and direct radiative perturbations by species and source type, *Geophys. Res. Lett.*, *32*, L12803, doi:10.1029/2004GL021743.

Redemann, J., R. P. Turco, K. N. Liou, P. V. Hobbs, W. S. Hartley, R. W. Bergstrom, E. V. Browell, and P. B. Russell (2000), Case studies of the vertical structure of the direct shortwave aerosol radiative forcing during TARFOX, *J. Geophys. Res.*, *105*(D8), 9971–9979.

Redemann, J., P. Pilewskie, P. B. Russell, J. M. Livingston, S. Howard, B. Schmid, J. Pommier, W. Gore, J. Eilers, and M. Wendisch (2006), Airborne measurements of spectral direct aerosol radiative forcing in the Intercontinental Chemical Transport Experiment/Intercontinental Transport and Chemical Transformation of anthropogenic pollution 2004, *J. Geophys. Res.*, *111*, D14210, doi:10.1029/2005JD006812.

Reid, J. S., P. V. Hobbs, R. J. Ferek, D. R. Blake, J. V. Martins, M. R. Dunlap, and C. Liousse (1998), Physical, chemical and optical properties of regional hazes dominated by smoke in Brazil, *J. Geophys. Res.*, *103*(D24), 32,059–32,080.

Reid, J. S., R. Koppmann, T. F. Eck, and D. P. Eleuterio (2005a), A review of biomass burning emissions part II: Intensive physical properties of biomass burning particles, *Atmos. Chem. Phys.*, *5*, 799–825.

Reid, J. S., T. F. Eck, S. A. Christopher, R. Koppmann, O. Dubovik, D. P. Eleuterio, B. N. Holben, E. A. Reid, and J. Zhang (2005b), A review of biomass burning emissions part III: Intensive optical properties of biomass burning particles, *Atmos. Chem. Phys.*, *5*, 827–849.

Remer, L. A., et al. (2005), The MODIS aerosol algorithm, products and validation, *J. Atmos. Sci.*, *62*, 947–973.

Ross, J. L., P. V. Hobbs, and B. Holben (1998), Radiative characteristics of regional hazes dominated by smoke from biomass burning in Brazil: Closure tests and direct radiative forcing, *J. Geophys. Res.*, *103*(D24), 31,925–31,941.

Russell, P. B., et al. (2002), Comparison of aerosol single scattering albedos derived by diverse techniques in two North Atlantic experiments, *J. Atmos. Sci.*, *59*, 609–619.

Schmid, B., et al. (2003), Coordinated airborne, spaceborne, and ground-based measurements of massive, thick aerosol layers during the dry season in southern Africa, *J. Geophys. Res.*, *108*(D13), 8496, doi:10.1029/2002JD002297.

Schmid, B., et al. (2006), How well do state-of-the-art techniques measuring the vertical profile of tropospheric aerosol extinction compare?, *J. Geophys. Res.*, *111*, D05S07, doi:10.1029/2005JD005837.

Schwartz, S. E. (2004), Uncertainty requirements in radiative forcing of climate change, *J. Air Waste Manage. Assoc.*, *54*, 1351–1359.

Seinfeld, J. H., and S. N. Pandis (1998), *Atmospheric Chemistry and Physics: From Air Pollution to Climate Change*, 1326 pp., John Wiley, Hoboken, N. J.

Sheridan, P. J., et al. (2005), The Reno Aerosol Optics Study: An evaluation of aerosol absorption measurement methods, *Aerosol Sci. Technol.*, *29*, 1–16.

Sierau, B., D. S. Covert, D. J. Coffman, P. K. Quinn, and T. S. Bates (2006), Aerosol optical properties during the 2004 New England Air Quality Study–Intercontinental Transport and Chemical Transformation: Gulf of Maine surface measurements—Regional and case studies, *J. Geophys. Res.*, *111*, D23S37, doi:10.1029/2006JD007568.

Sinha, P., P. V. Hobbs, R. J. Yokelson, I. T. Bertschi, D. R. Blake, I. J. Simpson, S. Gao, T. W. Kirchstetter, and T. Novakov (2003a), Emissions of trace gases and particles from savanna fires in southern Africa, *J. Geophys. Res.*, *108*(D13), 8487, doi:10.1029/2002JD002325.

Sinha, P., P. V. Hobbs, R. J. Yokelson, D. R. Blake, S. Gao, and T. W. Kirchstetter (2003b), Distributions of trace gases and aerosols during the dry biomass burning season in southern Africa, *J. Geophys. Res.*, *108*(D17), 4536, doi:10.1029/2003JD003691.

Sinha, P., L. Jaegle, P. V. Hobbs, and Q. Liang (2004), Transport of biomass burning emissions from southern Africa, *J. Geophys. Res.*, *109*, D20204, doi:10.1029/2004JD005044.

Stein, D. C., R. J. Swap, S. Greco, S. J. Piketh, S. A. Macko, B. G. Doddridge, T. Elias, and R. T. Bruintjes (2003), Haze layer characterization and associated meteorological controls along the eastern coastal region of southern Africa, *J. Geophys. Res.*, *108*(D13), 8506, doi:10.1029/2002JD003237.

Swap, R. J., and P. D. Tyson (1999), Stable discontinuities as determinants of the vertical distribution of aerosols and trace gases in the atmosphere, *S. Afr. J. Sci.*, *95*, 63–71.

Swap, R. J., H. J. Annegarn, J. T. Suttles, M. D. King, S. Platnick, J. L. Privette, and R. J. Scholes (2003), Africa burning: A thematic analysis of the Southern African Regional Science Initiative (SAFARI-2000), *J. Geophys. Res.*, *108*(D13), 8465, doi:10.1029/2003JD003747.

Thekaekara, M. P. (1973), Solar energy outside the earth's atmosphere, *Sol. Energy*, *14*, 109–127.

Thompson, A. M., J. C. Witte, M. T. Freiman, N. A. Phahlane, and G. J. R. Coetzee (2002), Lusaka, Zambia, during SAFARI-2000: Convergence of local and imported ozone pollution, *Geophys. Res. Lett.*, *29*(20), 1976, doi:10.1029/2002GL015399.

Thompson, A. M., et al. (2003), Southern Hemisphere Additional Ozonesondes (SHADOZ) 1998–2000 tropical ozone climatology: 1. Comparison with Total Ozone Mapping Spectrometer (TOMS) and ground-based measurements, *J. Geophys. Res.*, *108*(D2), 8238, doi:10.1029/2001JD000967.

Thompson, T. M. (2004), 5. Halocarbons and other atmospheric trace species, in *Summary Rep. 27, 2002–2003*, pp. 115–133, edited by R. C. Schnell, A.-M. Buggle, and R. M. Rosson, Global Monit. Div., Earth Syst. Res. Lab., NOAA, Boulder, Colo.

Vanhellemont, F., et al. (2005), A 2003 stratospheric aerosol extinction and PSC climatology from GOMOS measurements on Envisat, *Atmos. Chem. Phys.*, *5*, 2413–2417.

Wilks, D. S. (2006), *Statistical Methods in the Atmospheric Sciences*, 2nd ed., 627 pp., Academic, New York.

Wiscombe, W. J., and G. W. Grams (1976), The backscattered fraction in two-stream approximations, *J. Atmos. Sci.*, *33*, 2440–2451.

Yu, H., R. E. Dickinson, M. Chin, Y. J. Kaufman, M. Zhou, L. Zhou, Y. Tian, O. Dubovik, and B. N. Holben (2004), Direct radiative effect of aerosols as

determined from a combination of MODIS retrievals and GOCART simulations, *J. Geophys. Res.*, *109*, D03206, doi:10.1029/2003JD003914.

Yu, H., et al. (2006), A review of measurement-based assessments of the aerosol direct radiative effect and forcing, *Atmos. Chem. Phys.*, *6*, 613–666.

Zhou, M., H. Yu, R. E. Dickinson, O. Dubovik, and B. N. Holben (2005), A normalized description of the direct effect of key aerosol types on solar radiation as estimated from Aerosol Robotic Network aerosols and Moderate Resolution Imaging Spectroradiometer albedos, *J. Geophys. Res.*, *110*, D19202, doi:10.1029/2005JD005909.

Q. Fu, Department of Atmospheric Sciences, University of Washington, Seattle, WA 98195, USA.

B. I. Magi, Atmospheric and Oceanic Sciences Program, Princeton University, Princeton, NJ 08540, USA. (brian.magi@noaa.gov)

J. Redemann, Bay Area Environmental Research Institute, Sonoma, CA 95476, USA.

B. Schmid, Pacific Northwest National Laboratory, Richland, WA 99352, USA.